Available online at www.sciencedirect.com
ScienceDirect
Tectonophysics 461 (2008) 291–310
TECTONOPHYSICS
www.elsevier.com/locate/tecto

Ordovician–Silurian rift-passive margin on the Mexican margin of the Rheic Ocean overlain by Carboniferous–Permian periarc rocks: Evidence from the eastern Acatlán Complex, southern Mexico

Miguel Morales-Gámez [a], J. Duncan Keppie [a,*], Marc Norman [b]

[a] Departamento de Geología Regional, Instituto de Geología, Universidad Nacional Autónoma de México, C.P. 04510 México D.F., Mexico
[b] Research School of Earth Sciences, Australian National University, Mills Road, Building 61, Canberra, ACT 0200, Australia

Received 16 May 2007; received in revised form 22 October 2007; accepted 25 January 2008
Available online 8 February 2008

Abstract

In the Xayacatlán area of the Acatlán Complex in southern Mexico, several, N–S, fault-bounded packages of rocks occur (from west to east): (i) greenschist facies, interbedded psammites and pelites (Huerta Unit): the youngest concordant detrital zircon in the western part of the unit is 455±4 Ma; (ii) greenschist-amphibolite facies arkoses and psammites (Amate Unit): the youngest concordant detrital zircon gave a $^{206}Pb/^{238}U$ age of 902±14 Ma, and older concordant ages of ~900–1300 Ma; (iii) low grade clastic rocks and marbles (Permian Tecomate Formation); and (iv) greenschist facies psammites, pelites and thin tholeiitic mafic slices (Salada Unit): the youngest concordant detrital zircon yielded a $^{206}Pb/^{238}U$ age of 352±3 Ma and older concordant ages of ~434–485 Ma, 511–630 Ma, and 920–1200 Ma. The eastern part of the Huerta Unit is cut by pegmatite that yielded an almost concordant $^{206}Pb/^{238}U$ zircon age of 464±4 Ma (a mean age of the four almost concordant young zircons is ~485.5 Ma) interpreted as the time of intrusion, and inherited zircons with concordant ages of ~530–580 Ma and ~910–1200 Ma. These data suggest that the Huerta Unit ranges in age from Early (possibly older) to Late Ordovician. The Amate Unit is cut by granitic dikes, in which the youngest concordant $^{206}Pb/^{238}U$ zircon ages are 452±6 Ma and 447±3 Ma interpreted as the time of intrusion, and older inherited zircon ages with concordant $^{206}Pb/^{238}U$ ages in the range of 950–1250 Ma. The intrusive ages are similar to the 442±1 Ma concordant U–Pb age for mafic dikes that also cut the Amate Unit. These data constrain the depositional age of the Amate Unit between ~900 Ma and latest Ordovician. The age of the Salada Unit is probably Carboniferous because it is structurally overlain by the Lower–Middle Permian Tecomate Unit. The preponderance of 510–630 Ma and 900–1250 Ma ages in both the detrital and inherited ages in some of the dated samples suggests a source in the adjacent and subjacent Maya and Oaxacan Complex, respectively, although a xenocrystic host rock source cannot be ruled out for the intrusive rocks. The igneous intrusions have been interpreted as part of a 480–440 Ma bimodal rift-related suite. Their synchroneity with deposition of the Huerta Unit (and possibly also the Amate Unit) suggests a rift-passive margin environment of deposition on the southern margin of the Rheic Ocean. On the other hand, the Salada Unit and the Tecomate Formation appear to be synchronous with a Permo-Triassic magmatic arc that developed on the western margin of Pangea.

Keywords: Acatlán Complex; Mexico; Ordovician; Permo–Carboniferous; Geochronology

1. Introduction

The Xayacatlán area is located in the eastern part of the Acatlán Complex (Fig. 1) (designated the Mixteca terrane by Campa and Coney, 1983). The Acatlán Complex has been interpreted to be a vestige of a Paleozoic ocean, however, which ocean is presently a matter of debate. Ortega-Gutiérrez et al. (1999) suggested that it was part of the Cambro-Ordovician Iapetus Ocean, whereas Keppie and Ramos (1999) proposed that it was part of the Ordovician–Devonian Rheic Ocean. Subsequently, Talavera-Mendoza et al. (2005) and Vega-Granillo (2007) published a model that placed parts of the

* Corresponding author. Fax: +52 555 622 4290.
E-mail addresses: morzuz@yahoo.com (M. Morales-Gámez), duncan@servidor.unam.mx (J.D. Keppie).

0040-1951/$ - see front matter © 2008 Elsevier B.V. All rights reserved.
doi:10.1016/j.tecto.2008.01.014

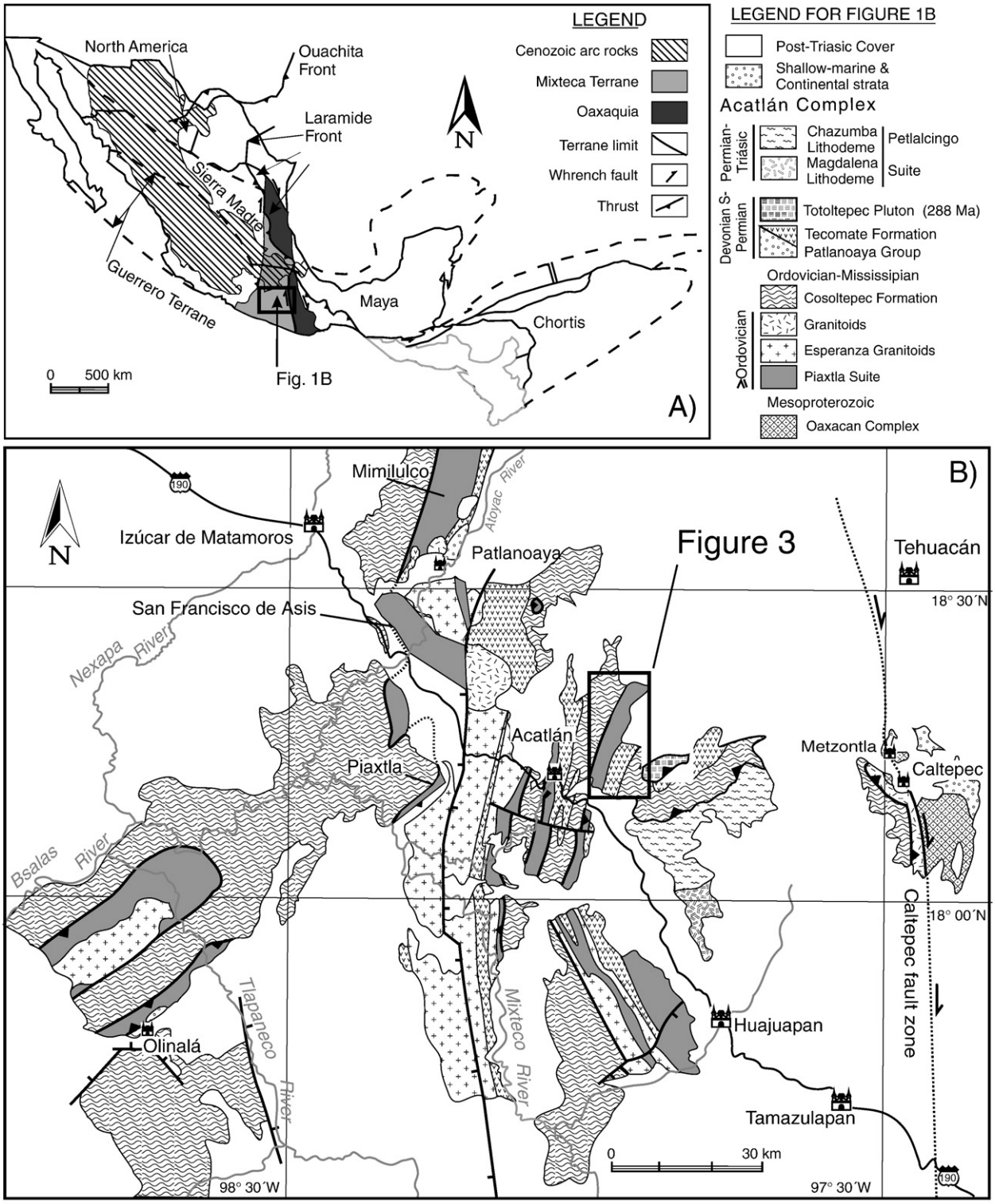

Fig. 1. Location of the Xayacatlán map shown on (A) terrane map of Middle America (modified after Keppie, 2004), and (B) geological map of the Acatlán Complex (modified after Keppie et al., 2006).

Acatlán Complex in three oceans: the El Rodeo unit and Lower Ordovician megacrystic granitoids were placed in the Bay Verte seaway between eastern Laurentia and an arc, the Xayacatlán Formation was attributed to the Iapetus Ocean, and the Cosoltepec Formation was envisaged as a passive margin bordering Amazonia. A recent synthesis by Keppie et al. (2008a) proposes that the Acatlán Complex originated on the southern margin of the Rheic Ocean traveling with Amazonia to

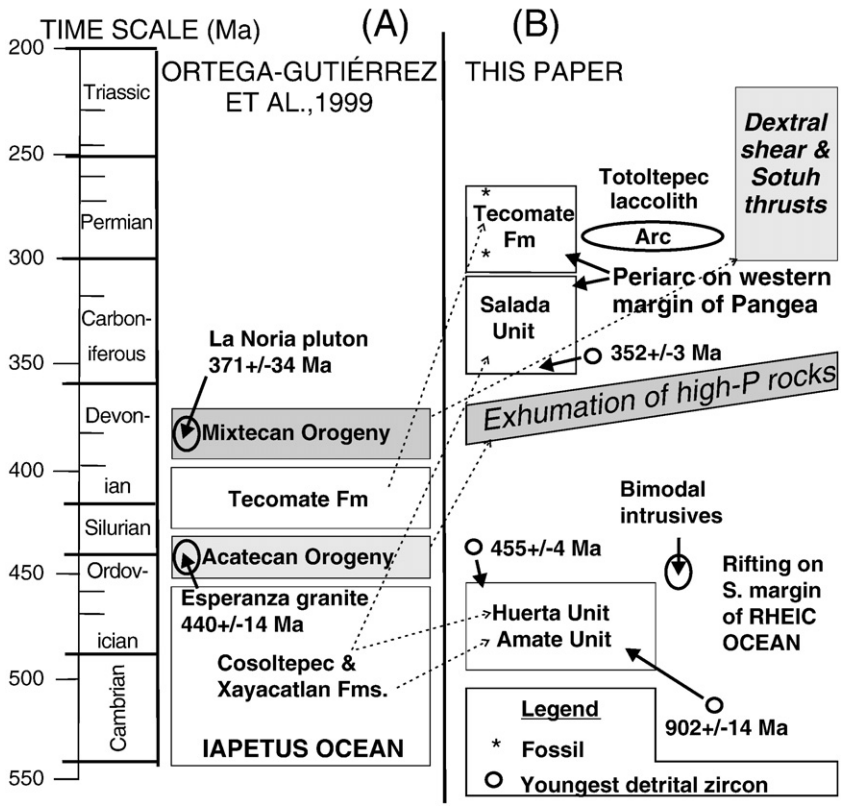

Fig. 2. Time-and-space diagram showing geological record of the Xayacatlán area: (A) after Ortega-Gutiérrez et al. (1999), and (B) this work.

end up on the active margin of the paleo-Pacific Ocean (Keppie et al., 2008a).

The Xayacatlán area is critical to resolution of this debate because it is the type area of the Xayacatlán Formation (Ortega-Gutiérrez, 1975). Ortega-Gutiérrez (1975) described the Xayacatlán Formation as an assemblage of metapsammites, metapelites, metagabbros, amphibolites, and serpentinite associated with megacrystic granitoids (Esperanza granitoids) that had undergone eclogite facies metamorphism (Fig. 2A). This high pressure metamorphism was believed to be late Ordovician based on the inference that the megacrystic granitoids were decompression melts that yielded a lower intercept U–Pb age of 440±14 Ma (Ortega-Gutiérrez et al., 1999). During this tectonothermal event, the Xayacatlán Formation was believed to have been thrust over the low grade Petlalcingo Group consisting of the Magdalena Migmatite at the base, the Chazumba Formation, and the Cosoltepec Formation at the top. Following exhumation, these rocks were unconformably overlain by the Tecomate Formation (of supposedly Siluro-Devonian age), which was intruded by arc-related rocks of Devonian age (based on a lower intercept age of 371±34 Ma (poorly defined lower intercept U–Pb TIMS zircon age: Yañez et al., 1991) during a Middle–Upper Devonian orogeny called the Mixtecan Orogeny (Sánchez-Zavala et al., 2000). This was followed by deposition of Carboniferous and Permian rocks unconformably on the older rocks.

However, the eclogite facies metamorphism has since been dated directly as Mississippian in the northern part of the Acatlán Complex (Middleton et al., 2007; Elías-Herrera et al., 2007), whereas the megacrystic granitoids are almost exclusively of Ordovician age (Sánchez-Zavala et al., 2004; Talavera-Mendoza et al., 2005; Miller et al., 2007). Furthermore, the fossils and dated granitic pebbles in Tecomate Formation show it to be Early–Middle Permian, possibly extending into the Carboniferous in undated underlying rocks (Keppie et al., 2004a). The Magdalena and Chazumba units contain detrital zircons as young as Permian and Triassic, whereas the youngest detrital zircons in units included in the Cosoltepec Formation of the eastern Acatlán Complex are either Ordovician (~455 Ma: Keppie et al., 2004b, 2006) or Devono-Carboniferous (~410 and/or ~374 Ma: Talavera-Mendoza et al., 2005). This has led to a revision of the geological history of the Acatlán Complex that has been summarized by Nance et al. (2006, 2007) and Keppie et al. (2008a) involving:

(i) deposition of ?Cambro-Ordovician rift-passive margin sediments associated with intrusion of bimodal, rift-related igneous rocks (Miller et al., 2007; Keppie et al., 2008b; Ramos-Arias et al., 2008);
(ii) deposition of latest Devonian–Permian–Triassic continental-shallow marine rocks (Vachard et al., 2000) that was synchronous with Mississippian exhumation of the high pressure rocks (Middleton et al., 2007), extensional and dextral shear on listric normal zones and N–S vertical zones (Elías-Herrera and Ortega-Gutiérrez, 2002; Ramos-Arias et al., 2008), and Permo-Triassic arc magmatism (Torres et al., 1999; Malone et al., 2002).

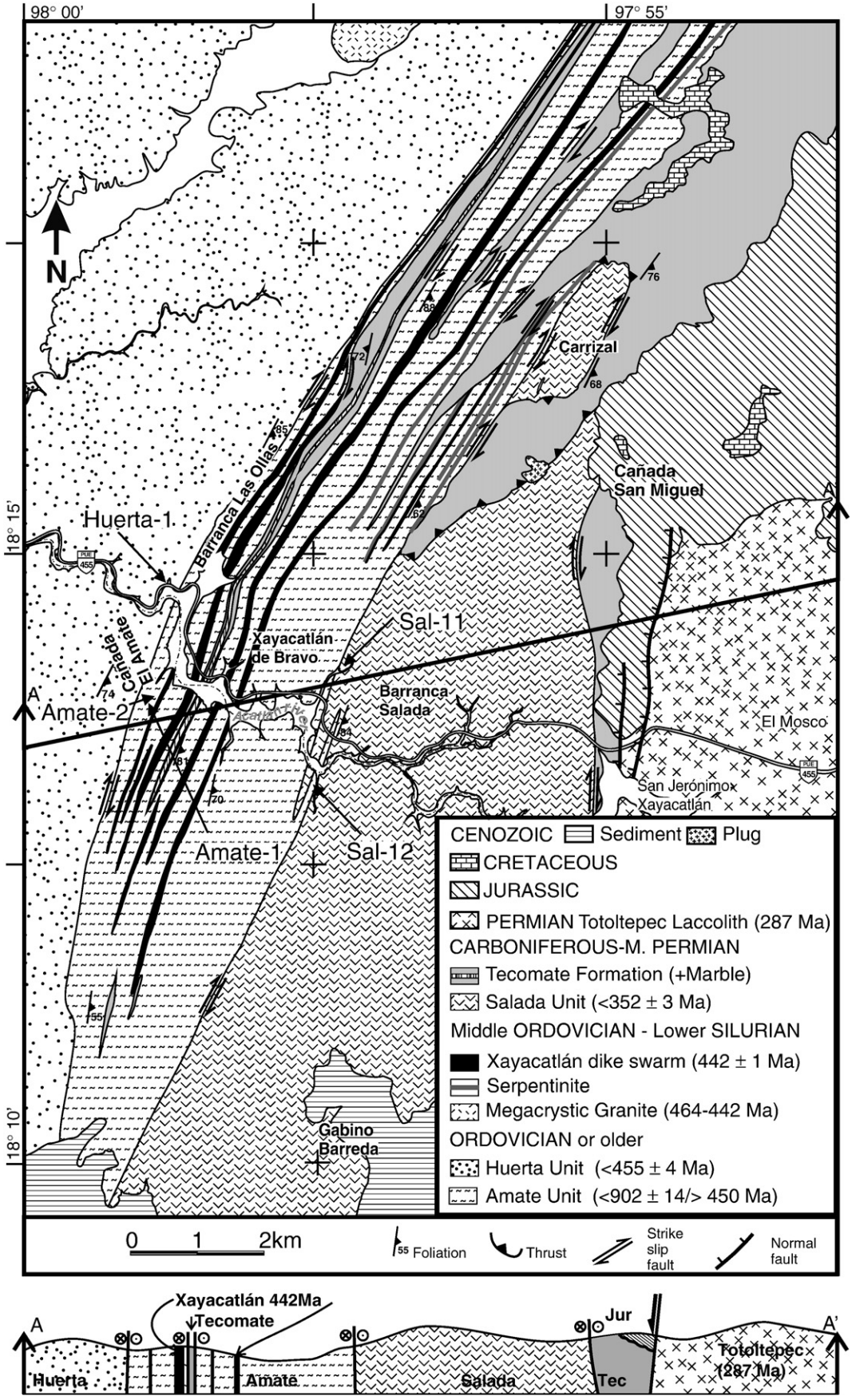

Fig. 3. Geological map of the Xayacatlán area.

Table 1
U–Pb LA-ICPMS analyses of zircons in a pegmatite sample in the Xayacatlán area, Acatlán Complex, southern Mexico: HUERTA-1 (see Fig. 3 for sample locations)

Sample/analysis	$^{206}Pb/^{238}U$	Percentage error	$^{207}Pb/^{235}U$	Percentage error	$^{207}Pb/^{206}Pb$	Percentage error	Age, Ma $^{206}Pb/^{238}U$	(2σ)	$^{207}Pb/^{235}U$	(2σ)	$^{207}Pb/^{206}Pb$	(2σ)
HUERTA-1												
ap05e10rim	0.1079	0.00086	0.9355	0.0092	0.06287	0.00062	659	10	671	10	702	42
ap05e11core	0.1513	0.00123	1.4791	0.0213	0.07091	0.00078	908	14	922	17	954	44
ap05e12	0.197	0.0014	2.297	0.0372	0.08458	0.00132	1150	19	1211	23	1304	60
ap05e13	0.0912	0.0007	0.7578	0.0213	0.06028	0.00189	565	14	573	25	612	134
ap05e14	0.117	0.0007	1.0857	0.0125	0.06732	0.00077	708	9	746	12	846	48
ap05e15	0.0913	0.00041	0.7574	0.0081	0.06019	0.00062	563	5	573	9	610	44
ap05e16	0.1127	0.00034	0.9879	0.0056	0.0636	0.00035	687	4	698	6	728	22
ap05f05	0.4287	0.0021	9.4091	0.0452	0.1592	0.00089	2299	20	2379	9	2446	20
ap05f06dark rim.	0.0938	0.0004	0.7637	0.0082	0.05907	0.00066	578	5	576	9	568	48
ap05f07mottled.core.	0.1249	0.00055	1.1849	0.0111	0.06883	0.00062	757	7	794	10	892	38
ap05f08	0.0855	0.00037	0.686	0.0062	0.05819	0.00056	529	5	530	7	536	40
ap05f09	0.0905	0.0009	0.7327	0.0155	0.05873	0.00143	563	16	558	18	556	106
ap05f10	0.3966	0.00238	8.5912	0.0481	0.15713	0.00074	2160	25	2296	10	2424	16
ap05f11	0.1165	0.00076	1.0801	0.0095	0.06726	0.00057	710	9	744	9	844	34
ap05f12	0.1746	0.00066	1.8474	0.0176	0.07673	0.00071	1036	8	1063	12	1114	38
ap05f13	0.1006	0.00056	0.8499	0.0097	0.0613	0.00067	617	7	625	11	648	48
ap05f14	0.0897	0.00045	0.7378	0.0081	0.05963	0.00069	554	6	561	9	590	50
ap05f15	0.0778	0.00036	0.6137	0.0071	0.05724	0.00065	483	5	486	9	500	50
ap05f16	0.4805	0.00221	12.3109	0.0665	0.18584	0.00095	2531	21	2628	10	2704	18
ap05g05	0.1732	0.00132	1.8143	0.0318	0.07599	0.00131	1030	16	1051	23	1094	70
ap05g06	0.092	0.00036	0.8328	0.0082	0.06569	0.00064	563	5	615	9	796	42
ap05g07	0.1685	0.00113	1.9705	0.0211	0.08484	0.00088	997	13	1105	14	1310	40
ap05g08	0.0933	0.00081	0.777	0.0184	0.06041	0.00154	575	10	584	21	618	110
ap05g09	0.1516	0.00091	1.4613	0.0178	0.06991	0.00073	911	11	915	15	924	44
ap05g10d.rim	0.08	0.00035	0.6243	0.0066	0.05662	0.00061	496	4	493	8	476	48
ap05g11l.core	0.0804	0.00042	0.6502	0.0075	0.05864	0.00071	499	5	509	9	552	52
ap05g12	0.1042	0.00048	0.9385	0.0135	0.06536	0.00093	636	6	672	14	784	60
ap05g13	0.1057	0.00035	0.9022	0.0076	0.06193	0.00053	648	4	653	8	670	36
ap05g14	0.0937	0.00046	0.7813	0.0111	0.06048	0.00084	576	5	586	13	620	60
ap05g15	0.0904	0.00098	0.8729	0.0357	0.07007	0.00294	551	13	637	39	930	174
ap05g16	0.3259	0.00147	4.9909	0.0359	0.11108	0.00083	1820	18	1818	12	1816	28
ap05h05	0.2037	0.00065	2.2638	0.0152	0.08062	0.00052	1197	8	1201	9	1212	26
ap05h06	0.0851	0.00083	0.6911	0.0254	0.05889	0.00225	529	11	533	31	562	168
ap05h07	0.1748	0.00072	1.9479	0.0265	0.08084	0.00104	1030	9	1098	18	1216	52
ap05h08	0.205	0.00133	3.628	0.0395	0.12836	0.001	1205	15	1556	17	2074	28
ap05h09	0.18	0.00074	1.8704	0.0172	0.07538	0.00077	1069	9	1071	12	1078	40
ap05h10	0.1713	0.00081	1.7546	0.0223	0.07428	0.00091	1021	10	1029	16	1048	48
ap05h11	0.0746	0.00031	0.5913	0.0052	0.05748	0.00051	464	4	472	7	510	38
ap05h12	0.1381	0.00062	1.3176	0.009	0.06923	0.00046	832	8	853	8	904	28
ap05h13	0.0962	0.00047	0.787	0.0127	0.05935	0.00095	591	6	589	14	580	70
ap05h14	0.1546	0.00056	1.5503	0.0116	0.07273	0.00051	920	7	951	9	1006	28
ap05h15	0.095	0.00065	0.7901	0.0145	0.06036	0.00113	583	11	591	16	616	82
ap05h16	0.1179	0.00101	1.0652	0.024	0.06556	0.00146	716	12	736	24	792	94
ap05i05	0.4544	0.00204	11.5921	0.0545	0.18502	0.00104	2396	21	2572	9	2698	18
ap05i06	0.2908	0.00125	4.1756	0.0263	0.10415	0.00055	1645	14	1669	10	1698	20
ap05i07	0.2028	0.0014	2.2418	0.0365	0.08017	0.00135	1189	18	1194	23	1200	68
ap05i08	0.0686	0.00045	0.569	0.0075	0.06017	0.00079	427	6	457	10	608	56
ap05i09	0.1699	0.00093	1.7583	0.0222	0.07508	0.00104	1009	12	1030	16	1070	56
ap05i10	0.5104	0.00327	16.3265	0.1339	0.23201	0.00174	2614	32	2896	16	3064	22
ap05i11	0.1769	0.00115	1.8844	0.0249	0.07727	0.00104	1051	14	1076	18	1128	54
ap05i12	0.0732	0.00063	0.605	0.0097	0.05995	0.00098	453	9	480	12	600	72
ap05i13core	0.1549	0.0009	1.5343	0.023	0.07183	0.00119	924	11	944	18	980	68
ap05i14rim	0.0875	0.00044	0.7191	0.0065	0.05964	0.00052	541	5	550	8	590	38
ap05i15	0.1966	0.00077	2.1807	0.0177	0.08047	0.00058	1156	9	1175	11	1208	28
ap05i16	0.0909	0.00035	0.7429	0.0079	0.05929	0.00065	562	4	564	9	576	48
ap05j05	0.3835	0.0013	6.8902	0.0496	0.13033	0.00083	2092	13	2097	13	2102	22
ap05j06	0.1625	0.00065	1.8017	0.0092	0.08042	0.00039	971	8	1046	7	1206	20
ap05j07	0.177	0.00074	1.8419	0.0151	0.07546	0.00057	1052	9	1061	11	1080	30
ap05j08	0.1283	0.00059	1.2004	0.0096	0.06786	0.00058	771	7	801	9	864	34
ap05j09	0.0876	0.00084	0.7361	0.011	0.06093	0.00101	535	10	560	13	636	70
ap05j10	0.2448	0.00118	3.5992	0.0328	0.10666	0.00094	1399	13	1549	14	1742	32

(continued on next page)

Table 1 (*continued*)

Sample/analysis	$^{206}Pb/^{238}U$	Percentage error	$^{207}Pb/^{235}U$	Percentage error	$^{207}Pb/^{206}Pb$	Percentage error	Age, Ma $^{206}Pb/^{238}U$	(2σ)	$^{207}Pb/^{235}U$	(2σ)	$^{207}Pb/^{206}Pb$	(2σ)
HUERTA-1												
ap05j11	0.0907	0.00079	0.6987	0.0234	0.05588	0.0018	561	11	538	28	446	142
ap05j12	0.0908	0.00047	0.7568	0.0104	0.06045	0.00081	560	6	572	12	618	58
ap05j13core	0.108	0.00048	0.8978	0.0086	0.06027	0.00064	661	6	651	9	612	46
ap05j14rim	0.101	0.00051	0.8343	0.007	0.0599	0.00053	619	6	616	8	598	38
ap05j15	0.1678	0.00057	1.7281	0.0137	0.07468	0.00062	999	7	1019	10	1058	34
ap05j16	0.0949	0.0005	0.7955	0.0086	0.06077	0.00067	584	6	594	10	630	48

(iii) a tectonothermal event during the Jurassic that may be related to a mantle plume (Keppie et al., 2004b);
(iv) deposition of Mesozoic platformal rocks and Cenozoic arc-related rocks.

Our reexamination of the Xayacatlán area involving mapping and zircon geochronology shows that: (i) whereas some of the units are Ordovician or older others are post-Devonian (probably Carboniferous and Permian); (ii) high grade (amphibolite facies) metamorphism is restricted to syntectonic gabbroic intrusions and their contact aureoles intruded during transtensional deformation (none of the rocks have undergone eclogite facies metamorphism); and (iii) most of the N–S striking contacts between the units are vertical shear zones (not thrusts as previously inferred). These data are then applied to paleogeographic reconstructions and we suggest that whereas the Ordovician rocks formed on the southern margin of the Rheic Ocean, the Carboniferous and Permian rocks formed on the active Pacific margin of Pangea.

2. Xayacatlán area

The Xayacatlán area was originally mapped by Ortega-Gutiérrez (1975), who recognized two units: retrograded eclogites of the Xayacatlán Formation that was thrust over the low grade Cosoltepec Formation (Fig. 2A). The Xayacatlán Formation was subsequently included in the eclogitic Piaxtla Group (Ramírez-Espinosa, 2001) and renamed the Piaxtla Suite by Middleton et al. (2007). However, the absence of eclogite facies metamorphism in the Xayacatlán area makes its inclusion in the Piaxtla Suite uncertain. Furthermore, correlation of the low grade rocks in the vicinity of Xayacatlán with the type Cosoltepec Formation are also uncertain because detrital zircon suites have different ages (c.f. Talavera-Mendoza et al., 2005; Keppie et al., 2006). In view of these problems, we define new names for most of the units in the Xayacatlán area (Figs. 2B and 3). The structure, metamorphism and geochemistry of the various units forms part of separate papers (e.g. Keppie et al., 2008b).

2.1. Huerta Unit (new name)

The Huerta Unit occurs with a N–S trending fault block that is bounded on its western side by sub-greenschist facies rocks assigned to the Tecomate Formation, and on its eastern side by rocks of the Amate Unit where the contact is a dextral shear zone formed under greenschist facies metamorphic conditions (Fig. 3). A megacrystic granite is exposed along the northern margin of the Xayacatlán area, however, its contact with the Huerta Unit is not exposed. It is composed of interbedded metapsammites and metapelites consisting of quartz, muscovite, chlorite and accessory zircon and opaque minerals. The unit is pervasively intruded by veins that gradually change in mineralogy from quartz veins in the west to pegmatites in the east. All of these rocks have undergone intense polyphase deformation at least three sets of folds including sheath folds under greenschist facies metamorphic conditions (Malone et al., 2002; and paper in preparation by authors). In view of this, it is impossible to measure a type section. However, the road between Xayacatlán and Acatlán provides an excellent cross-section of the unit. A sample from the western part of this unit has yielded detrital zircons, the youngest of which yielded a concordant age of 455±4 Ma with older population age peaks at ~600 Ma and ~1–1.2 Ga (Keppie et al., 2006). A pegmatite sample (Fig. 3: HUERTA-1: 18°14.758′, 97° 58.727′) was collected in the eastern part of the fault block for U–Pb detrital zircon analysis (Fig. 3).

2.2. Amate Unit (new name)

The Amate Unit occurs in the central N–S trending fault block (Fig. 3). All the contacts with other rock units are dextral shear zones. The Amate Unit is mainly composed of metaarkose, metapsammite, and metapelite that are intruded by mafic and felsic dikes. The metasedimentary rocks generally consist of quartz, muscovite, feldspar, and chlorite with accessory zircon and opaque minerals. However, adjacent to the largest mafic dike, the rocks are hornfelsed and contain large decussate muscovite and clinozoisite crystals. The petrography, geochemistry and geochronology of the mafic (gabbro and diabase) and felsic (granite and pegmatite) rocks have been described by Keppie et al. (2008b). They are mainly mafic amphibolitic gneisses with ultramafic and anorthositic bands with a continental tholeiitic signature cut by medium grained mafic dikes and granitic pegmatites. In places, these mafic dikes have undergone intense shearing associated with retrogressive metamorphism that produced serpentinite and chlorite schist. The rocks of the Amate Unit have been deformed by at least three sets of folds generally developed under greenschist facies metamorphic conditions (detailed in a paper in preparation by authors). As a

Table 2
U–Pb LA-ICPMS analyses of zircons in a metapsammite sample of the Amate Unit in the Xayacatlán area, Acatlán Complex, southern Mexico: AMATE-1 (see Fig. 3 for sample locations)

Sample/analysis	$^{206}Pb/^{238}U$	Percentage error	$^{207}Pb/^{235}U$	Percentage error	$^{207}Pb/^{206}Pb$	Percentage error	Age, Ma $^{206}Pb/^{238}U$	(2σ)	$^{207}Pb/^{235}U$	(2σ)	$^{207}Pb/^{206}Pb$	(2σ)
AMATE-1												
ap03h05	0.1959	0.0007	2.1751	0.0126	0.08053	0.0005	1151	8	1173	8	1208	26
ap03h06	0.2068	0.0008	2.3453	0.0178	0.08225	0.0005	1211	9	1226	11	1250	26
ap03h07	0.151	0.0005	1.4568	0.0079	0.06998	0.0003	906	6	913	6	926	18
ap03h08	0.2138	0.0011	2.4633	0.0227	0.08357	0.0009	1248	12	1261	13	1282	40
ap03h09	0.1692	0.0009	1.767	0.0186	0.07573	0.0008	1006	10	1033	14	1088	42
ap03h10	0.1823	0.0011	1.8743	0.0337	0.07456	0.0013	1079	12	1072	24	1056	70
ap03h11	0.1542	0.0018	1.4552	0.0469	0.06845	0.0025	923	21	912	39	882	154
ap03h12	0.1664	0.0007	1.6448	0.0176	0.07169	0.0008	992	8	988	13	976	44
ap03h13	0.1592	0.0006	1.5677	0.0121	0.07142	0.0005	953	8	958	10	968	28
ap03h14	0.2091	0.0017	2.4126	0.0396	0.0837	0.0012	1222	18	1246	24	1284	56
ap03h15	0.1965	0.0008	2.1623	0.0132	0.07982	0.0006	1157	9	1169	8	1192	28
ap03h16	0.1589	0.0006	1.683	0.0076	0.07679	0.0003	952	7	1002	6	1114	16
ap03i05	0.1716	0.0009	1.7676	0.017	0.0747	0.0007	1021	10	1034	12	1060	36
ap03i06	0.1805	0.0008	1.8891	0.0134	0.0759	0.0004	1069	9	1077	9	1092	24
ap03i07	0.1723	0.0007	1.7778	0.0135	0.07482	0.0006	1025	8	1037	10	1062	30
ap03i08	0.1642	0.0022	1.908	0.0277	0.08429	0.0004	978	26	1084	19	1298	20
ap03i09	0.1902	0.0012	2.1003	0.0269	0.0801	0.0011	1120	15	1149	18	1198	56
ap03i10	0.1501	0.0012	1.4315	0.0269	0.06916	0.0013	900	14	902	22	902	78
ap03i11	0.1411	0.0006	1.3589	0.0121	0.06987	0.0007	847	7	871	10	924	38
ap03i12	0.195	0.0013	2.1476	0.0288	0.07987	0.0011	1147	15	1164	19	1192	54
ap03i13	0.1945	0.0007	2.1055	0.0116	0.07849	0.0004	1147	7	1151	8	1158	20
ap03i14	0.2046	0.0014	2.2091	0.0258	0.07832	0.0009	1205	15	1184	16	1154	48
ap03i15	0.1725	0.0006	1.7495	0.0121	0.07357	0.0005	1027	6	1027	9	1028	26
ap03i16	0.2112	0.0009	2.4046	0.0137	0.08257	0.0005	1235	9	1244	8	1258	24
ap03j05	0.2149	0.0012	2.3879	0.0224	0.08061	0.0008	1256	13	1239	14	1210	38
ap03j06	0.1877	0.0008	2.0741	0.0091	0.08015	0.0003	1111	8	1140	6	1200	14
ap03j07	0.2015	0.0007	2.2795	0.0125	0.08206	0.0004	1180	8	1206	8	1246	20
ap03j08	0.1536	0.0008	1.61	0.0079	0.076	0.0003	924	10	974	6	1094	20
ap03j09	0.156	0.0011	1.5346	0.0273	0.07136	0.0014	933	13	944	22	966	78
ap03j10	0.2282	0.0009	2.7648	0.0182	0.08789	0.0006	1325	9	1346	10	1380	26
ap03j11	0.1699	0.0007	1.7146	0.0111	0.0732	0.0006	1013	8	1014	8	1018	32
ap03j12	0.1724	0.0009	1.8003	0.0247	0.07573	0.0011	1025	10	1046	18	1086	58
ap03j13	0.2011	0.0007	2.1895	0.0204	0.07898	0.0008	1182	8	1178	13	1170	40
ap03j14	0.1894	0.002	2.0413	0.0274	0.07818	0.0008	1116	22	1129	18	1150	40
ap03j15	0.1698	0.0005	1.7364	0.0099	0.07417	0.0004	1011	6	1022	7	1046	22
ap03j16	0.1585	0.0011	1.5431	0.0201	0.07064	0.0009	948	12	948	16	946	50
ap03k05	0.1932	0.0007	2.1011	0.0118	0.07887	0.0004	1138	8	1149	8	1168	20
ap03k06	0.1832	0.0008	1.9052	0.0105	0.07543	0.0005	1084	9	1083	7	1078	26
ap03k07	0.156	0.0009	1.5089	0.0243	0.07017	0.0013	936	11	934	20	932	76
ap03k08	0.1702	0.0012	1.7423	0.0211	0.07427	0.0008	1013	14	1024	16	1048	44
ap03k09	0.1854	0.0008	1.9556	0.0198	0.07651	0.0008	1098	9	1100	14	1108	42
ap03k10	0.1921	0.0008	2.0666	0.0118	0.07803	0.0004	1134	9	1138	8	1146	22
ap03k11	0.1968	0.0006	2.4169	0.0126	0.0891	0.0003	1151	7	1248	7	1406	14
ap03k12	0.1721	0.0007	1.7297	0.0164	0.0729	0.0007	1024	8	1020	12	1010	40
ap03k13	0.1743	0.0005	1.7838	0.01	0.07421	0.0004	1036	6	1040	7	1046	20
ap03k14	0.1678	0.0007	1.6805	0.0096	0.07264	0.0004	1000	7	1001	7	1004	22
ap03k15	0.1896	0.0009	2.1294	0.023	0.08147	0.0009	1116	10	1158	15	1232	46
ap03k16	0.2207	0.0009	2.6476	0.0191	0.08701	0.0006	1285	10	1314	11	1360	24
ap03l05	0.1697	0.001	1.7163	0.0156	0.07335	0.0006	1010	11	1015	12	1022	34
ap03l06	0.1762	0.0011	1.8235	0.0352	0.07506	0.0015	1049	14	1054	25	1070	82
ap03l07	0.1596	0.0008	1.6017	0.0178	0.07277	0.0008	951	10	971	14	1006	48
ap03l08	0.1578	0.0006	1.5676	0.0152	0.07207	0.0008	945	7	957	12	986	42
ap03l09	0.1877	0.0008	2.187	0.0103	0.08451	0.0004	1105	10	1177	7	1304	16
ap03l10	0.2089	0.0008	2.3823	0.0157	0.08273	0.0006	1223	9	1237	9	1262	26
ap03l11	0.2148	0.0009	2.5011	0.0133	0.08446	0.0004	1251	11	1272	8	1302	20
ap03l12	0.1756	0.0008	1.7631	0.0153	0.07282	0.0006	1043	9	1032	11	1008	32
ap03l13	0.1649	0.0016	1.6489	0.0424	0.07253	0.002	985	19	989	32	1000	110
ap03l14	0.2224	0.0009	3.5857	0.0384	0.11693	0.0012	1243	15	1546	17	1908	36
ap03l15	0.158	0.001	1.5318	0.0201	0.07031	0.0008	946	12	943	16	936	48
ap03l16	0.143	0.001	1.4067	0.0255	0.07133	0.0013	856	12	892	22	966	78

(continued on next page)

Table 2 (*continued*)

Sample/analysis	$^{206}Pb/^{238}U$	Percentage error	$^{207}Pb/^{235}U$	Percentage error	$^{207}Pb/^{206}Pb$	Percentage error	Age, Ma $^{206}Pb/^{238}U$	(2σ)	$^{207}Pb/^{235}U$	(2σ)	$^{207}Pb/^{206}Pb$	(2σ)
AMATE-1												
ap03m05	0.1631	0.0007	1.6395	0.009	0.07289	0.0003	974	8	986	7	1010	16
ap03m06	0.1874	0.0014	1.9049	0.037	0.07371	0.0014	1106	16	1083	26	1032	76
ap03m07	0.1751	0.0012	1.7998	0.0149	0.07455	0.0008	1040	14	1045	11	1056	46
ap03m08	0.1663	0.0008	1.7034	0.0121	0.07428	0.0005	988	10	1010	9	1048	28
Ap03m09	0.2021	0.0012	2.1879	0.0234	0.07851	0.0008	1187	13	1177	15	1158	42
Ap03m10	0.2232	0.0008	2.5847	0.0194	0.08398	0.0006	1299	9	1296	11	1292	26
Ap03m11	0.2099	0.0011	2.3755	0.0283	0.08207	0.0009	1228	12	1235	17	1246	44
Ap03m12	0.1701	0.0007	1.7071	0.0142	0.0728	0.0007	1012	9	1011	11	1008	38
Ap03m13	0.2032	0.0009	2.2199	0.0173	0.07925	0.0007	1192	10	1187	11	1178	38
Ap03m14	0.2012	0.001	2.1713	0.0154	0.07826	0.0005	1184	12	1172	10	1152	28
Ap03m15	0.1607	0.0014	1.5535	0.0259	0.0701	0.0014	963	17	952	21	930	80
Ap03m16	0.2001	0.0009	2.228	0.0118	0.08077	0.0004	1175	11	1190	7	1214	18
Ap03n05	0.2141	0.001	2.4366	0.0239	0.08255	0.0008	1252	12	1253	14	1258	36
Ap03n06	0.1834	0.0007	1.955	0.0174	0.07732	0.0007	1082	9	1100	12	1128	34
Ap03n07	0.1494	0.0006	1.5046	0.0129	0.07302	0.0006	896	8	932	10	1014	34
Ap03n08	0.2004	0.001	2.2346	0.0183	0.08087	0.0006	1176	11	1192	11	1218	30
Ap03n09	0.1472	0.0005	1.471	0.0078	0.07246	0.0004	884	6	919	6	998	24
Ap03n10	0.1924	0.0009	2.1696	0.0165	0.08178	0.0006	1120	12	1171	11	1240	28
Ap03n11	0.1547	0.0011	1.5071	0.0213	0.07064	0.001	926	13	933	17	946	56
Ap03n12	0.173	0.0007	1.7662	0.014	0.07404	0.0005	1029	9	1033	10	1042	30
Ap03n13	0.2089	0.0008	2.3261	0.017	0.08074	0.0006	1221	9	1220	10	1214	28
Ap03n14	0.1688	0.0012	1.6488	0.0251	0.07085	0.0013	1006	14	989	19	952	78
Ap03n15	0.1709	0.0007	1.7168	0.011	0.07285	0.0005	1017	9	1015	8	1008	26
Ap03n16	0.1749	0.001	1.7606	0.0178	0.07302	0.0009	1039	12	1031	13	1014	50

consequence of the polyphase deformation, no stratigraphic section is available for a type section: the Amate River provides the best section of the unit (Fig. 3). Three samples were collected for U–Pb zircon analyses (Fig. 3): one from a feldspathic psammite (AMATE-1, 18° 13.793′, 97° 58.965′), and the other two from cross-cutting foliated granitic dikes (AMATE-2: 18° 13.772′, 97° 58.963′; SAL-12: 18°13.247′, 97° 57.608′).

2.3. Salada Unit (new name)

The Salada Unit occurs in a N–S trending fault block in the eastern part of the area. It is bounded on its western side by a dextral shear zone that juxtaposes it against the Tecomate Formation, on its northern side by an E–W trending, shallow N-dipping shear zone, above which lies the Tecomate Formation, and to the south it is unconformably overlain by Cenozoic rocks (Fig. 3). It consists mainly of metapelites, metapsammites and thin, tectonically intercalated mafic lenses. The metasedimentary rocks made up of quartz, muscovite, chlorite and accessory opaque minerals. The mafic rocks are composed of amphibole, chlorite, feldspar, epidote and accessory opaque minerals. A metapsammite sample was collected for U–Pb zircon analysis (Fig. 3: SAL-11: 18° 14.077′, 97° 57.341′).

2.4. Tecomate Formation

The Tecomate Formation in the Xayacatán area is tectonically juxtaposed against all the previously described units, either along N–S trending dextral shear zones or above gently N-dipping shear zones with gently N-plunging stretching lineations (Malone et al., 2002; paper in preparation by authors) (Fig. 3). In the north, it is overlain unconformably by Mesozoic rocks, whereas in the southeast it is faulted against the Totoltepec laccolith (Fig. 3). The Tecomate Formation consists predominantly of meta-arkoses, metapsammites, slates, metaconglomerates, and marbles. The clastic rocks consist mainly of quartz, feldspar, muscovite, chlorite, epidote and opaque minerals. The conglomerates contain a diverse assemblage of pebbles: granitoid and volcanic rocks, metapsammite, and vein quartz. Granitoid pebbles from a conglomerate ~20 km to the east of the Xayacatlán area have yielded U–Pb ages of ~290 Ma and are inferred to have been derived from the Lower Permian Totoltepec laccolith (Yañez et al., 1991; Keppie et al., 2004b), which is exposed along the eastern margin of Fig. 3. On the other hand, marbles in the type section of the Tecomate Formation exposed to the south of the town of Acatlán (Fig. 1B), have yielded latest Pennsylvanian–Early Permian microfossils (Keppie et al., 2004a). Deformation in the Tecomate Formation in the Xayacatlán area varies from almost undeformed to polyphase involving three sets of folds (Malone et al., 2002; and paper in preparation by authors). The grade of metamorphism varies from sub-greenschist facies to lower greenschist facies (Malone et al., 2002).

2.5. Totoltepec laccolith

The Totoltepec laccolith crops out along the eastern margin of the Xayacatlán area (Fig. 3). It has yielded concordant U–Pb zircon ages of ~288 Ma (Yañez et al. et al., 1991; Keppie et al.,

Table 3
U–Pb LA-ICPMS analyses of zircons in a granitic dike cutting the Amate Unit in the Xayacatlán area, Acatlán Complex, southern Mexico: AMATE-2 (see Fig. 3 for sample locations)

Sample/analysis	$^{206}Pb/^{238}U$	Percentage error	$^{207}Pb/^{235}U$	Percentage error	$^{207}Pb/^{206}Pb$	Percentage error	Age, Ma $^{206}Pb/^{238}U$	(2σ)	$^{207}Pb/^{235}U$	(2σ)	$^{207}Pb/^{206}Pb$	(2σ)
AMATE-2												
Ap05k05	0.0737	0.0006	0.5643	0.013	0.05554	0.00118	457	8	454	17	434	94
Ap05k06	0.2138	0.0014	2.5109	0.0271	0.0852	0.00085	1252	17	1275	16	1318	38
Ap05k07	0.0745	0.0005	0.5894	0.0136	0.05741	0.00134	462	7	470	17	506	104
Ap05k08	0.0717	0.0002	0.5543	0.0022	0.05606	0.0002	447	3	448	3	454	16
Ap05k09	0.071	0.0002	0.5598	0.0029	0.05721	0.00027	444	3	451	4	498	20
ap05k10	0.0808	0.0004	0.74	0.0081	0.06646	0.00073	495	5	562	10	820	46
ap05k11	0.1871	0.0007	2.0692	0.0174	0.08023	0.00054	1102	8	1139	11	1202	26
ap05k12	0.0702	0.0004	0.525	0.0104	0.05427	0.00112	437	6	428	14	382	92
ap05k13	0.071	0.0006	0.5561	0.018	0.05677	0.00194	442	8	449	23	482	152
ap05k14	0.2115	0.0013	2.3549	0.0162	0.08077	0.00058	1235	15	1229	10	1214	30
ap05k15	0.2128	0.0008	2.4141	0.0176	0.08227	0.00064	1244	9	1247	11	1250	30
ap05k16	0.1794	0.0012	1.838	0.0298	0.07432	0.00115	1061	14	1059	21	1050	62
ap05l05	0.1579	0.0012	1.5687	0.0207	0.07205	0.00104	944	14	958	16	986	60
ap05l06	0.192	0.0013	2.0882	0.0232	0.0789	0.00082	1132	15	1145	15	1168	40
ap05l07	0.1708	0.0006	1.8449	0.0116	0.07833	0.00052	1018	7	1062	8	1154	26
ap05l08	0.072	0.0003	0.6143	0.0045	0.0619	0.00048	447	4	486	6	670	32
ap05l09	0.0723	0.0003	0.5715	0.0034	0.05729	0.00037	449	3	459	4	502	28
ap05l10	0.1523	0.001	1.5168	0.0155	0.07226	0.00059	914	12	937	13	992	32
ap05l11	0.1588	0.0008	1.5635	0.0152	0.07139	0.00066	950	9	956	12	968	38
ap05l12	0.0734	0.0004	0.5574	0.0093	0.05505	0.00088	458	5	450	12	414	70
ap05l13	0.0709	0.0005	0.5503	0.0144	0.05628	0.00154	442	7	445	19	462	122
ap05l14	0.0693	0.0005	0.5402	0.0077	0.05653	0.00083	432	6	439	10	472	64
ap05l15	0.1225	0.0006	1.187	0.0094	0.07028	0.00067	745	7	795	9	936	38
ap05l16	0.073	0.0006	0.6545	0.0107	0.06506	0.0007	451	7	511	13	776	46
ap05m05	0.0706	0.0006	0.5539	0.013	0.05688	0.0014	440	8	448	17	486	110
ap05m06rim	0.0744	0.0002	0.5863	0.0029	0.05713	0.00026	462	3	469	4	496	20
ap05m07core	0.1217	0.0005	1.118	0.0111	0.06662	0.00061	740	6	762	11	824	38
ap05m08	0.1343	0.0006	1.2545	0.0133	0.06777	0.00072	809	7	825	12	860	44
ap05m09	0.0764	0.0004	0.6006	0.0069	0.05702	0.00064	476	5	478	9	492	50
ap05m10	0.1674	0.0007	1.6782	0.0123	0.07272	0.00057	997	8	1000	9	1006	30
ap05m11	0.1959	0.0009	2.143	0.0238	0.07936	0.00084	1154	10	1163	15	1180	40
ap05m12	0.2101	0.0007	2.3772	0.0138	0.08205	0.00053	1230	8	1236	8	1246	26
ap05m13	0.0711	0.0004	0.5631	0.0091	0.05743	0.00097	442	5	454	12	508	74
ap05m14	0.0723	0.0005	0.5602	0.0103	0.05617	0.00112	450	6	452	13	458	88
ap05m15	0.1639	0.0006	1.6294	0.0116	0.0721	0.00055	978	7	982	9	988	32
ap05m16	0.2099	0.0009	2.3427	0.0225	0.08096	0.00075	1228	11	1225	14	1220	36
ap05n05	0.0279	0.0003	0.2063	0.0069	0.05365	0.00193	177	4	190	12	356	162
ap05n06	0.1935	0.0016	2.1068	0.0356	0.07898	0.00132	1140	19	1151	23	1170	66
ap05n07	0.1923	0.0013	2.1478	0.0247	0.08099	0.00081	1134	15	1164	16	1220	40
ap05n08	0.0694	0.0004	0.5338	0.0075	0.05582	0.00087	433	5	434	10	444	68
ap05n09	0.0697	0.0007	0.5297	0.0122	0.05515	0.00116	435	9	432	16	418	94
ap05n10	0.071	0.0004	0.5539	0.0089	0.05658	0.00094	442	6	448	12	474	74
ap05n11	0.0697	0.0004	0.524	0.0088	0.05455	0.00087	434	6	428	12	392	72
ap05n12core	0.0705	0.0003	0.5318	0.006	0.0547	0.00066	439	4	433	8	400	54
ap05n13rim	0.0711	0.0003	0.5513	0.004	0.05621	0.00043	443	4	446	5	460	34
ap05n14rim	0.0749	0.0004	0.589	0.0074	0.05707	0.00074	466	5	470	9	494	58
ap05n15core	0.0709	0.0003	0.5573	0.0065	0.05705	0.00068	441	4	450	8	492	52
ap05n16	0.0962	0.0006	0.7973	0.0237	0.06012	0.00177	594	9	595	27	606	128
ap05o05	0.199	0.001	2.4302	0.0277	0.08856	0.00094	1163	12	1252	16	1394	40
ap05o06	0.1482	0.0014	1.387	0.0226	0.0679	0.00101	890	16	883	19	864	62
ap05o07	0.072	0.0003	0.5789	0.0042	0.05833	0.00043	447	4	464	5	542	32
ap05o08	0.1651	0.0009	1.6873	0.0202	0.07413	0.00089	985	11	1004	15	1044	48
ap05o09core	0.1955	0.001	2.1556	0.0181	0.07998	0.00078	1151	11	1167	12	1196	38
ap05o10rim	0.0725	0.0003	0.6449	0.0104	0.06451	0.00095	447	4	505	13	758	62
ap05o11core	0.1599	0.0012	1.583	0.0258	0.07179	0.00116	954	15	964	20	978	66
ap05o12rim	0.0742	0.0003	0.6091	0.0044	0.05957	0.00042	459	3	483	6	586	30

2004b). It varies from mafic (hornblende, epidote, chlorite) to felsic (quartz, feldspar, muscovite) and has a calc-alkaline geochemistry interpreted in terms of arc magmatism (Malone et al., 2002). The laccolith contains a folded foliation with a N-plunging mineral lineation interpreted in terms of syntectonic intrusion during S-vergent thrusting (Malone et al., 2002).

Table 4
U–Pb LA-ICPMS analyses of zircons in a metapsammite sample of the Salada Unit in the Xayacatlán area, Acatlán Complex, southern Mexico: SAL-12 (see Fig. 3 for sample locations)

Sample/analysis	$^{206}Pb/^{238}U$	Percentage error	$^{207}Pb/^{235}U$	Percentage error	$^{207}Pb/^{206}Pb$	Percentage error	Age, Ma $^{206}Pb/^{238}U$	(2σ)	$^{207}Pb/^{235}U$	(2σ)	$^{207}Pb/^{206}Pb$	(2σ)
SAL-12												
ap05a05	0.1393	0.0006	1.3007	0.0144	0.06772	0.00076	839	7	846	13	860	46
ap05a06	0.0753	0.0003	0.5968	0.0034	0.05745	0.0003	468	4	475	4	508	24
ap05a07	0.074	0.0004	0.5933	0.0043	0.05818	0.00048	460	5	473	5	536	36
ap05a08	0.2085	0.0008	2.3722	0.0119	0.08254	0.00043	1224	9	1234	7	1258	20
ap05a09	0.0745	0.0004	0.5829	0.0078	0.05674	0.00073	463	5	466	10	480	56
ap05a10	0.0497	0.0004	0.4598	0.0051	0.06704	0.00052	313	6	384	7	838	32
ap05a11	0.2053	0.0008	2.2962	0.017	0.08112	0.0005	1204	9	1211	10	1224	24
ap05a12	0.1712	0.0007	1.7477	0.0147	0.07406	0.00069	1019	8	1026	11	1042	36
ap05a13	0.2104	0.0007	2.3278	0.0242	0.08023	0.00081	1232	8	1221	15	1202	40
ap05a14	0.0737	0.0003	0.579	0.0058	0.05695	0.00056	459	4	464	7	488	44
ap05a15	0.0746	0.0003	0.5904	0.0045	0.05744	0.0004	463	4	471	6	508	30
ap05a16	0.0741	0.0003	0.6635	0.0064	0.06495	0.00066	456	3	517	8	772	42
ap05b05	0.2104	0.001	2.3768	0.0209	0.08195	0.00074	1231	11	1236	13	1244	34
ap05b06	0.2014	0.0009	2.2188	0.0131	0.07991	0.00051	1184	11	1187	8	1194	24
ap05b07	0.0761	0.0004	0.6075	0.0046	0.05791	0.00043	473	5	482	6	526	34
ap05b08	0.1744	0.001	1.7986	0.0214	0.0748	0.00102	1035	12	1045	16	1062	56
ap05b09	0.158	0.0008	1.5908	0.0232	0.07301	0.00103	946	9	967	18	1014	58
ap05b10	0.0751	0.0003	0.6156	0.0057	0.05947	0.00056	466	4	487	7	584	42
ap05b11	0.2019	0.001	2.2455	0.0171	0.08068	0.00058	1186	11	1195	11	1212	28
ap05b12	0.1151	0.0008	1.0693	0.0145	0.0674	0.00096	683	11	738	14	850	58
ap05b13	0.1384	0.001	1.581	0.0207	0.08288	0.001	822	12	963	16	1266	46
ap05b14	0.1368	0.0009	1.3218	0.0169	0.07008	0.00102	822	11	855	15	930	60
ap05b15	0.0759	0.0003	0.6231	0.006	0.05958	0.00058	469	3	492	8	588	42
ap05b16core	0.091	0.0007	0.8237	0.0078	0.06565	0.00069	560	9	610	9	794	44
ap05c05rim	0.0887	0.0003	0.808	0.0051	0.06604	0.00045	543	4	601	6	806	28
ap05c06	0.0748	0.0003	0.6124	0.0044	0.05936	0.00047	463	4	485	6	580	34
ap05c07	0.0723	0.0004	0.616	0.0056	0.06179	0.00048	448	5	487	7	666	34
ap05c08main zone	0.0694	0.0005	0.7175	0.0067	0.075	0.00053	424	7	549	8	1068	28
ap05c09rim?	0.0728	0.0002	0.5733	0.0038	0.05715	0.00037	452	3	460	5	496	28
ap05c10	0.0711	0.0003	0.9512	0.009	0.09711	0.0009	422	6	679	9	1568	36
ap05c11	0.078	0.0004	0.6415	0.0061	0.05967	0.00061	482	5	503	8	590	44
ap05c12	0.0783	0.0003	0.6511	0.0077	0.0603	0.00072	486	4	509	9	614	50
ap05c13	0.1697	0.0008	1.8473	0.0168	0.07896	0.00076	1001	9	1062	12	1170	36
ap05c14core	0.0726	0.0004	0.5647	0.0067	0.05639	0.00061	452	6	455	9	466	48
ap05c15rim	0.0735	0.0004	0.5659	0.008	0.05582	0.00078	457	5	455	10	444	60
ap05c16	0.1299	0.0011	1.287	0.0257	0.07189	0.00129	765	15	840	23	982	74
ap05d05	0.1661	0.0005	1.6569	0.0101	0.07236	0.00045	991	6	992	8	994	26
ap05d06	0.0743	0.0003	0.5738	0.006	0.05603	0.00054	463	4	460	8	452	44
ap05d07	0.1822	0.0011	1.9441	0.0247	0.07741	0.00098	1076	13	1096	17	1130	50
ap05d08	0.0721	0.0003	0.6582	0.0047	0.06622	0.00045	445	4	514	6	812	28
ap05d09	0.1518	0.0008	1.4925	0.0161	0.07132	0.00081	912	9	927	13	966	46
ap05d10	0.0737	0.0003	0.7233	0.0073	0.0712	0.00077	451	4	553	9	962	44
ap05d11	0.2747	0.0012	3.7626	0.026	0.09936	0.00062	1565	12	1585	11	1612	22
ap05d12	0.2208	0.0012	2.606	0.0305	0.08561	0.00104	1280	14	1302	17	1328	48
ap05d13	0.0747	0.0003	0.5832	0.0045	0.05662	0.0004	465	4	467	6	476	32
ap05d14	0.0746	0.0004	0.586	0.0064	0.05697	0.00063	463	5	468	8	490	48
ap05d15	0.1821	0.001	2.0148	0.025	0.08025	0.00101	1076	12	1121	17	1202	48
ap05d16	0.0743	0.0004	0.5703	0.0094	0.05567	0.00097	463	5	458	12	438	76
ap05e05	0.0764	0.0003	0.7428	0.0065	0.07055	0.00068	467	4	564	8	944	38
ap05e06	0.0741	0.0004	0.5804	0.0059	0.05677	0.00052	461	5	465	8	482	40
ap05e07	0.149	0.0004	1.4563	0.0063	0.0709	0.00026	895	5	912	5	954	16
ap05e08	0.1832	0.0008	2.2745	0.015	0.09004	0.0005	1077	9	1204	9	1426	22
ap05e09	0.0735	0.0003	0.8316	0.0063	0.08209	0.00065	444	5	615	7	1246	30

2.6. Jurassic conglomerate

Lying unconformably upon the Tecomate Formation in the northeastern part of the area are a sequence of red conglomerates, sandstones and occasional shaly layers (Fig. 3). Leaf impressions recovered from this sequence are probably Jurassic (R. Weber, pers. comm., 2005). The conglomerates contain pebbles of schist and large feldspar and quartz grains. These

Table 5
U–Pb LA-ICPMS analyses of zircons in a granitic dike cutting the Amate Unit in the Xayacatlán area, Acatlán Complex, southern Mexico: SAL.11 (see Fig. 3 for sample locations)

Sample/analysis	$^{206}Pb/^{238}U$	Percentage error	$^{207}Pb/^{235}U$	Percentage error	$^{207}Pb/^{206}Pb$	Percentage error	Age, Ma $^{206}Pb/^{238}U$	(2σ)	$^{207}Pb/^{235}U$	(2σ)	$^{207}Pb/^{206}Pb$	(2σ)
SAL-11												
ap03a05	0.5925	0.0023	19.7945	0.0673	0.24231	0.00073	3000	19	3081	7	3134	8
ap03a06	0.1097	0.0005	0.9668	0.0079	0.0639	0.00048	671	6	687	8	738	32
ap03a07	0.1689	0.0006	1.7389	0.0144	0.07468	0.00063	1008	7	1023	11	1058	34
ap03a08	0.1997	0.0013	2.3	0.0455	0.08352	0.00159	1174	16	1212	28	1280	74
ap03a09	0.5024	0.0022	11.8614	0.0474	0.17123	0.00067	2628	19	2594	8	2568	14
ap03a10	0.098	0.0005	0.8209	0.0069	0.06076	0.00058	602	6	609	8	630	42
ap03a11	0.0871	0.0005	0.7168	0.0116	0.05967	0.00092	538	6	549	14	590	68
ap03a12	0.1045	0.0005	0.8922	0.0062	0.06194	0.00046	641	5	648	7	670	32
ap03a13	0.3512	0.0012	12.1767	0.0426	0.25151	0.0007	1940	11	2618	7	3194	10
ap03a14	0.2776	0.0012	4.1555	0.0258	0.10858	0.00073	1566	13	1665	10	1774	26
ap03a15	0.0851	0.0006	0.7059	0.0077	0.06015	0.00067	527	8	542	9	608	48
ap03a16	0.0973	0.0005	0.7968	0.01	0.05942	0.00078	599	6	595	11	582	58
ap03b05	0.134	0.0007	1.2375	0.0099	0.06697	0.00051	812	8	818	9	836	32
ap03b06	0.3057	0.002	5.1402	0.0334	0.12198	0.00059	1717	21	1843	11	1984	16
ap03b07	0.3356	0.0012	5.2714	0.0285	0.11394	0.00062	1869	13	1864	9	1862	20
ap03b08	0.1777	0.0009	1.8322	0.0114	0.07479	0.0004	1055	11	1057	8	1062	20
ap03b09	0.2049	0.0008	2.3866	0.0155	0.0845	0.00046	1198	8	1239	9	1304	22
ap03b10	0.14	0.0006	1.3963	0.0101	0.07235	0.00046	839	7	887	8	994	26
ap03b11	0.1022	0.0004	0.8567	0.0072	0.06078	0.00051	629	5	628	8	630	36
ap03b12	0.2012	0.0008	2.1772	0.0155	0.0785	0.00057	1184	10	1174	10	1158	28
ap03b13	0.1025	0.0006	0.9125	0.0115	0.06455	0.00077	627	7	658	12	758	50
ap03b14	0.302	0.0009	4.4817	0.0134	0.10763	0.00042	1699	10	1728	5	1758	14
ap03b15	0.0829	0.0007	1.2626	0.0758	0.11048	0.00514	483	14	829	68	1806	168
ap03b16	0.2202	0.0084	16.4658	0.7014	0.54224	0.00672	492	220	2904	82	4000	0
ap03c05	0.1496	0.0047	2.9584	0.0846	0.14347	0.00194	847	60	1397	43	2268	46
ap03c06	0.1	0.0008	1.1146	0.0308	0.08087	0.00215	604	12	760	30	1218	104
ap03c07	0.1533	0.0007	1.493	0.0094	0.07063	0.00037	919	8	928	8	946	20
ap03c08	0.0724	0.0003	0.5811	0.0035	0.05823	0.00037	450	4	465	4	538	28
ap03c09	0.0617	0.0003	0.6057	0.0072	0.07117	0.00088	380	5	481	9	962	50
ap03c10	0.1779	0.0007	1.8184	0.0156	0.07413	0.00066	1056	9	1052	11	1044	36
ap03c11	0.0872	0.0004	0.7705	0.0065	0.06408	0.00062	544	5	580	7	744	42
ap03c12	0.3317	0.001	5.1702	0.0248	0.11305	0.00047	1848	10	1848	8	1848	16
ap03c13	0.1044	0.0005	0.991	0.0076	0.06884	0.00049	639	6	699	8	892	30
ap03c14	0.1481	0.0015	1.9885	0.0169	0.09736	0.00152	875	18	1112	11	1574	58
ap03c15	0.149	0.0006	1.7949	0.0179	0.0874	0.00087	876	8	1044	13	1368	38
ap03c16	0.065	0.0003	0.7303	0.0067	0.08152	0.00088	395	5	557	8	1232	42
ap03d05	0.0753	0.0002	0.5968	0.0054	0.05748	0.00056	469	3	475	7	508	42
ap03d06	0.0685	0.0004	0.5218	0.0078	0.05524	0.0008	434	7	426	10	422	66
ap03d07	0.0842	0.0004	0.6861	0.0096	0.05913	0.00079	521	6	530	12	570	58
ap03d08	0.1016	0.0005	0.8589	0.0071	0.06134	0.00059	624	7	630	8	650	40
ap03d09	0.1009	0.0005	0.8772	0.0113	0.06304	0.00093	620	6	639	12	708	64
ap03d10	0.5241	0.0023	13.6093	0.049	0.18836	0.00068	2710	21	2723	7	2726	12
ap03d11	0.0971	0.0006	0.8556	0.0076	0.06392	0.00062	597	7	628	8	738	40
ap03d12	0.1221	0.0004	1.0863	0.0086	0.06451	0.00049	742	5	747	8	758	32
ap03d13	0.1032	0.0007	0.9907	0.0141	0.06964	0.0011	626	9	699	14	916	66
ap03d14	0.1008	0.0004	0.8459	0.0087	0.06089	0.00062	621	5	622	10	634	44
ap03d15	0.0534	0.0003	0.4393	0.0066	0.05968	0.00089	334	4	370	9	592	66
ap03d16	0.0832	0.0012	0.9478	0.0181	0.08259	0.00249	500	16	677	19	1258	118
ap03e05	0.1246	0.0007	1.1595	0.0256	0.06749	0.00115	754	9	782	24	852	72
ap03e06	0.1456	0.0006	1.8269	0.011	0.09099	0.00056	885	8	1055	8	1446	24
ap03e07	0.1905	0.001	2.1608	0.0212	0.08227	0.00079	1122	12	1169	14	1250	38
ap03e08	0.0872	0.0004	0.7177	0.0093	0.05967	0.00083	539	5	549	11	590	60
ap03e09	0.3321	0.0024	8.2825	0.0654	0.1809	0.00166	1822	28	2262	14	2660	32
ap03e10	0.0824	0.0004	0.6537	0.0093	0.05755	0.00079	511	6	511	11	512	62
ap03e11	0.2037	0.0008	2.2611	0.0154	0.0805	0.00049	1195	10	1200	10	1208	24
ap03e12	0.056	0.0002	0.4169	0.0042	0.05398	0.00062	352	3	354	6	370	52
ap03e13	0.1016	0.0004	0.8675	0.0107	0.06192	0.00074	623	6	634	12	670	52
ap03e14	0.1165	0.0005	1.0567	0.0123	0.06581	0.00083	709	7	732	12	800	54
ap03e15	0.0736	0.0004	0.5859	0.0057	0.05772	0.00055	459	5	468	7	518	42
ap03e16	0.0783	0.0004	0.6278	0.007	0.05819	0.00066	485	5	495	9	536	50

(continued on next page)

Table 5 (*continued*)

Sample/analysis	$^{206}Pb/^{238}U$	Percentage error	$^{207}Pb/^{235}U$	Percentage error	$^{207}Pb/^{206}Pb$	Percentage error	Age, Ma $^{206}Pb/^{238}U$	(2σ)	$^{207}Pb/^{235}U$	(2σ)	$^{207}Pb/^{206}Pb$	(2σ)
SAL-11												
ap03f05	0.1581	0.0006	1.9772	0.0091	0.09068	0.00052	918	9	1108	6	1438	22
ap03f06	0.1646	0.0011	1.7427	0.0197	0.07677	0.0009	973	14	1024	15	1114	48
ap03f07	0.1534	0.0013	1.5557	0.0219	0.07355	0.00088	918	16	953	17	1028	48
ap03f08	0.1578	0.0006	1.6096	0.0106	0.074	0.00046	943	7	974	8	1040	26
ap03f09	0.1332	0.0012	1.2409	0.045	0.06758	0.00219	801	16	819	41	854	134
ap03f10	0.0992	0.0006	0.8582	0.0094	0.06278	0.00082	608	7	629	10	700	56
ap03f11	0.1048	0.0008	0.9372	0.0378	0.06487	0.00288	640	11	671	40	770	188
ap03f12	0.3579	0.0017	5.9463	0.0416	0.1205	0.00081	1974	19	1968	12	1962	24
ap03f13	0.203	0.0009	2.337	0.0236	0.08352	0.00071	1190	10	1224	14	1280	32
ap03f14	0.3538	0.0029	7.712	0.0671	0.15812	0.00059	1936	31	2198	16	2434	12
ap03f15	0.1801	0.0009	1.903	0.0124	0.07662	0.00056	1065	10	1082	9	1110	28
ap03f16	0.0887	0.0009	0.7442	0.0258	0.06085	0.0022	546	11	565	30	632	156
ap03g05	0.0908	0.0003	0.8468	0.007	0.06768	0.00057	554	5	623	8	858	34
ap03g06	0.0868	0.0006	0.7051	0.0113	0.05893	0.00098	536	7	542	13	564	74
ap03g07	0.0917	0.0005	0.7766	0.0077	0.06142	0.00073	566	6	584	9	652	50
ap03g08	0.0572	0.0002	0.4342	0.0066	0.05508	0.00089	358	3	366	9	414	72
ap03g09	0.0564	0.0002	0.4184	0.0033	0.05377	0.00042	352	3	355	5	360	36
ap03g10	0.0766	0.0004	0.6183	0.0098	0.05852	0.00105	476	6	489	12	548	80
ap03g11	0.0966	0.0005	0.8187	0.009	0.06146	0.00061	593	6	607	10	654	44
ap03g12	0.1022	0.0004	0.8782	0.0056	0.06234	0.00043	627	5	640	6	684	30
ap03g13	0.1485	0.0009	1.4725	0.0141	0.0719	0.00079	889	11	919	12	982	44
ap03g14	0.0916	0.0004	0.8903	0.0112	0.07052	0.00089	559	6	647	12	942	52
ap03g15	0.1826	0.0005	1.9295	0.0125	0.07664	0.00055	1082	6	1091	9	1110	30
ap03g16	0.3392	0.0013	5.4985	0.0302	0.11758	0.00061	1882	14	1900	9	1918	18

rocks are gently dipping to the north and post-date all but normal faulting.

3. LA-ICPMS zircon analyses

3.1. Analytical procedures

Preparation of the five samples was carried at Instituto de Geología, UNAM. About 15 kg of each of the selected samples for zircon dating was crushed with a jaw crusher and pulverized in a Bico disk mill. The heavy minerals were concentrated on a Wifley table and were then passed through a Frantz magnetic separator. A current up to 1.5 A is used to generate a magnetic field for samples to concentrate zircons suitable for LA-ICPMS dating. Further separation by passing non-magnetic fractions through heavy liquids (bromoform), ensured a nearly pure zircon concentration.

Zircons from all five samples were mounted in epoxy and polished for age determinations on individual grains by LA-ICPMS. All grains were photographed using transmitted and reflected light optical microscopy, and the internal structures of the grains imaged using SEM-CL. U–Pb isotopic compositions of individual zircon grains were determined at RSES-ANU, Canberra, Australia, using an ArF excimer laser system (193 nm, Lambda Physik) coupled to an Agilent 7500 quadrupole ICPMS (Eggins et al., 1998). Ablation was done under a He atmosphere in a custom-built sample chamber using a 40-micron diameter spot and a laser repetition rate of 4 Hz. Data were reduced relative to the reference zircon FC1 (1099 Ma, Paces and Miller 1993), with gas backgrounds collected before each analysis and subtracted from net intensities measured for each isotope. Internal precision of measured $^{207}Pb/^{206}Pb$ and $^{206}Pb/^{238}U$ ratios typically was ~0.5% 1σ relative standard deviation for individual analyses. The samples were analyzed in two sessions; replicate analyses of the FC1 zircon from each session indicate external reproducibilities of 0.9% ($n=30$) and 0.8% ($n=32$), respectively, on the measured $^{207}Pb/^{206}Pb$ ratios, 1.1% and 0.8%, respectively, on the measured $^{206}Pb/^{238}U$ ratios, and 1.2% and 1.6%, respectively, on the $^{208}Pb/^{232}Th$ ratios (1σ relative standard deviation). These errors are not included in the quoted uncertainties for individual analyses of the analyzed zircons. The data are provided in Tables 1–5 and the corrected $^{206}Pb/^{238}U$ data are plotted on Terra–Wasserburg diagrams (Figs. 4–8).

4. Results

A pegmatite cutting the eastern part of the Huerta Unit (HUERTA-1) consists of K-feldspar, quartz and muscovite with accessory zircon, apatite and opaque minerals. Zircons yielded $^{206}Pb/^{238}U$ ages ranging from 427 Ma to 2531 Ma, however the youngest, almost concordant $^{206}Pb/^{238}U$ zircon age is 464±4 Ma and a mean age of the four almost concordant young zircons is ~485.5 Ma (Fig. 4; Table 1): these are interpreted as dating the time of intrusion. Two population of older, inherited zircons with concordant ages have ages of ~530–580 Ma and ~910–1200 Ma.

Three samples were collected from the Amate Unit: one feldspathic metapsammite (AMATE-1) and two cross-cutting, foliated granitic dikes (AMATE-2 and SAL-12). The metapsammite is composed mainly of quartz, K-feldspar and muscovite. It yielded detrital zircons with $^{206}Pb/^{238}U$ ages ranging from 847 Ma to 1325 Ma, however, the youngest concordant detrital zircon gave

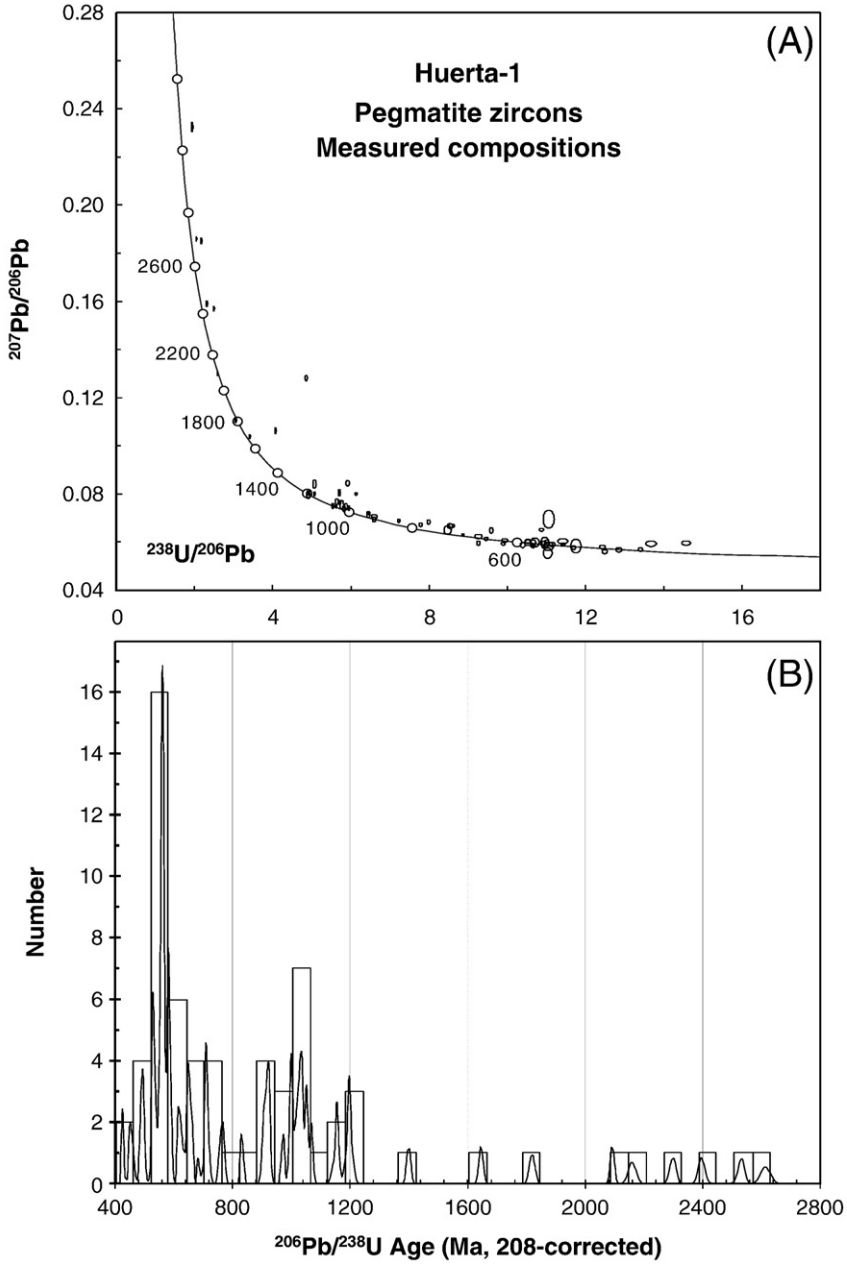

Fig. 4. U–Pb LA-ICPMS zircon analyses from pegmatite cutting the Huerta Unit (sample HUERTA-1) plotted on (A) a Terra–Wasserburg diagram, and (B) a histogram.

a $^{206}Pb/^{238}U$ age of 902±14 Ma, and older concordant ages in the range of ~900 Ma to 1300 Ma (Fig. 5: Table 2).

The foliated granite dike (AMATE-2) consists of quartz, feldspar, muscovite, and accessory zircon, apatite, and opaque minerals. The $^{206}Pb/^{238}U$ ages range from 432 Ma to 1252 Ma with the youngest concordant $^{206}Pb/^{238}U$ zircon age being 447± 3 Ma (Fig. 6, Table 3). Older inherited zircon ages with concordant $^{206}Pb/^{238}U$ ages in the range of 950–1230 Ma.

Another foliated and folded granitic dike (SAL-12) intruding the eastern part of the Amate Unit yielded $^{206}Pb/^{238}U$ zircon ages ranging from 422 Ma to 1565 Ma, however the youngest concordant age is 452±6 Ma interpreted as the time of intrusion (Fig. 7, Table 4). Older inherited zircons gave concordant $^{206}Pb/^{238}U$ ages in the range of 912–1280 Ma with single concordant ages at 839±7 Ma and 1565±12 Ma.

Detrital zircons in a metapsammite of the Salada Unit (SAL-11) yielded a $^{206}Pb/^{238}U$ ranging from 352 Ma to 3000 Ma with the youngest concordant detrital zircon yielded a $^{206}Pb/^{238}U$ age of 352±3 Ma (Fig. 8, Table 5). Older concordant ages of ~434–485 Ma, 511–630 Ma, and 920–1200 Ma.

5. Constraints on the ages of the new units

5.1. Huerta Unit

Deposition of the Huerta Unit is constrained by the 455±4 Ma age of the youngest detrital zircon (Keppie et al., 2006) and 464± 4 Ma intrusive age of a cross-cutting pegmatite. The ages are similar within analytical error and suggest that deposition was synchronous with intrusion. However, the two dated samples were collected

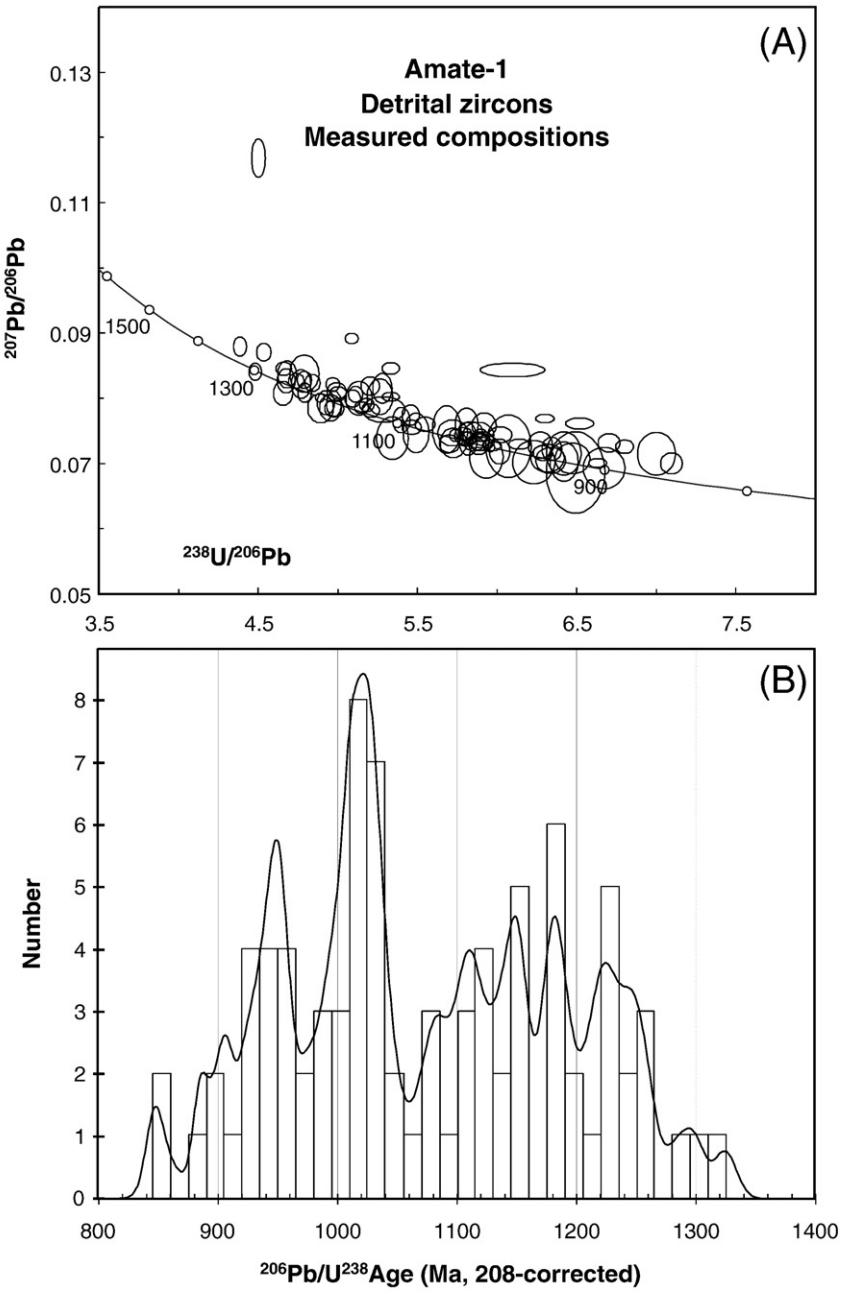

Fig. 5. U–Pb LA-ICPMS zircon analyses from metapsammite of the Amate Unit (sample AMATE-1) plotted on (A) a Terra–Wasserburg diagram, and (B) a histogram.

10 km apart from western and eastern parts of the Huerta Unit, respectively. Thus deposition of rocks in the eastern part of the unit that are cut by the pegmatite may be somewhat older than ~455 Ma. The polyphase deformation of the unit probably means that this problem cannot be ascertained by further mapping: further detrital zircon dating is required. Nevertheless, deposition of the unit probably took place during the Ordovician.

5.2. Amate Unit

Deposition of the Amate Unit is less tightly constrained: post-902±14 Ma (youngest concordant detrital zircon) and pre-447±3 Ma, pre-452±6 Ma (the intrusive ages of cross-cutting granite dikes: this paper), and pre-442±1 Ma (the intrusive age of a cross-cutting gabbro dike: Keppie et al., 2008b). The absence of late Neoproterozoic ages in the Amate Unit, where they are present in the Huerta Unit, suggests either that the units are of different ages or that the provenance changed. The latter situation is apparent in the Ordovician units of the Patlanoaya area (Keppie et al., 2008b) and in the Tecomate Formation (Sánchez-Zavala et al., 2004). However, at this stage, one cannot rule out a difference in the time of deposition.

5.3. Salada Unit

An older limit on the time of deposition of the Salada Unit is provided by the 352±3 Ma age of the youngest detrital zircon. A younger limit is not directly available. The Tecomate

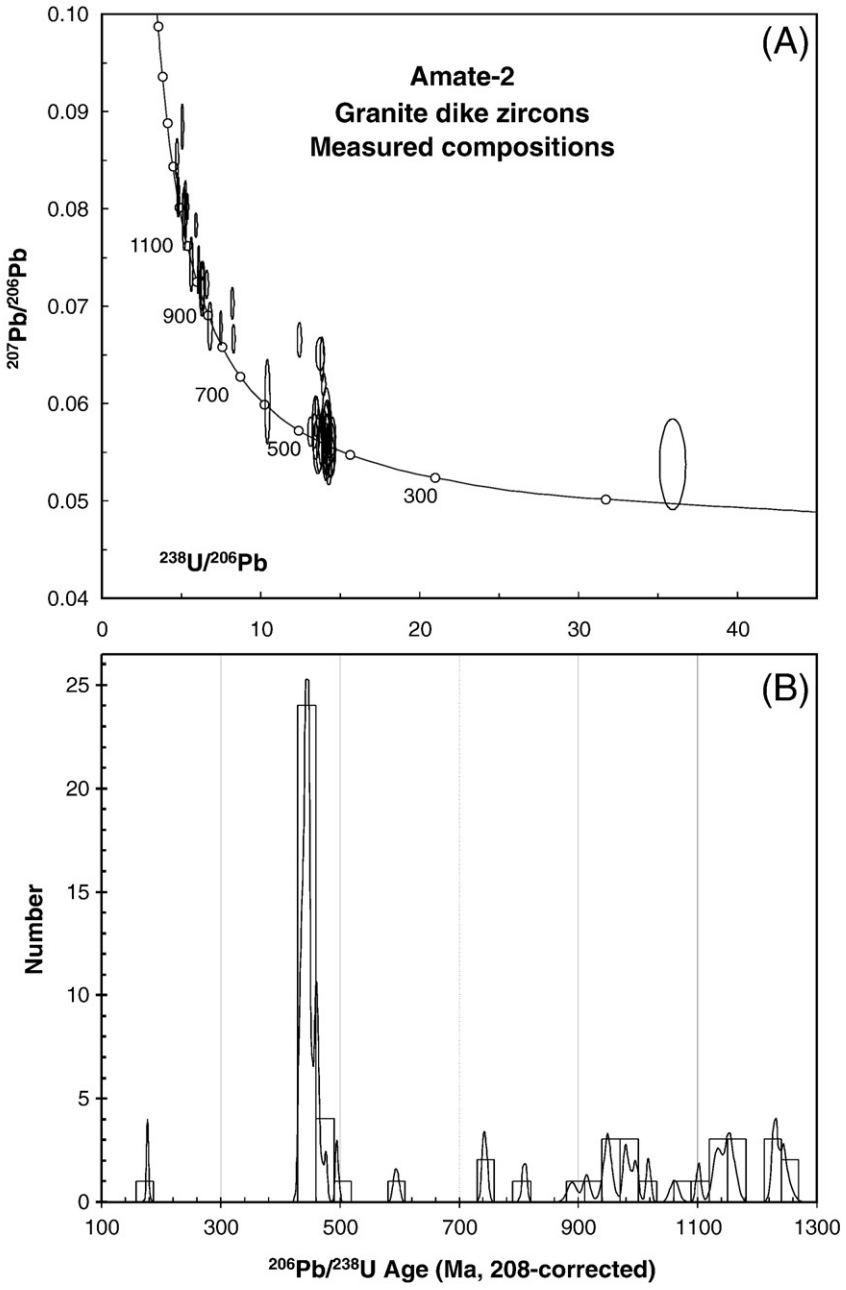

Fig. 6. U–Pb LA-ICPMS zircon analyses from granitic dike cutting the Amate Unit (sample AMATE-2) plotted on (A) a Terra–Wasserburg diagram, and (B) a histogram.

Formation is everywhere in tectonic contact with the Salada Unit, however, the lithologies are markedly distinct and the dated parts of the Tecomate Formation are latest Pennsylvanian to Middle Permian (Keppie et al., 2004a). Furthermore, it is lithologically distinct from the Permo-Triassic Chazumba and Magdalena units, which also have distinctly younger detrital zircon populations (Keppie et al., 2006). Thus its age is most likely to be Carboniferous.

6. Provenance of the detrital zircons

Whereas both the Huerta and Amate units both contain a 900–1300 Ma detrital zircon population, ~460 Ma and ~510–640 Ma populations are only recorded in the Huerta Unit. The 900–1300 Ma population is probably of local provenance in the neighbouring Oaxacan Complex (Fig. 1B), which has yielded ages ranging from 920 Ma to 1300 Ma (Keppie et al., 2003; Solari et al., 2003; Ortega-Obregón et al., 2003). A local source for the ~460 Ma detrital zircons is also likely in the Ordovician granitoids of the Acatlán Complex (Fig. 1B)(Sánchez-Zavala et al., 2004; Talavera-Mendoza et al., 2005; Miller et al., 2007). On the other hand a more distal source for the ~510–640 Ma zircons may be found in either the basement beneath the Yucatan Peninsula, the Brasiliano orogens of Amazonia, or Avalonia (which separated from Oaxaquia/Amazonia at ~480 Ma) (Keppie, 2004; Keppie et al., 2006; Nance et al., 2006).

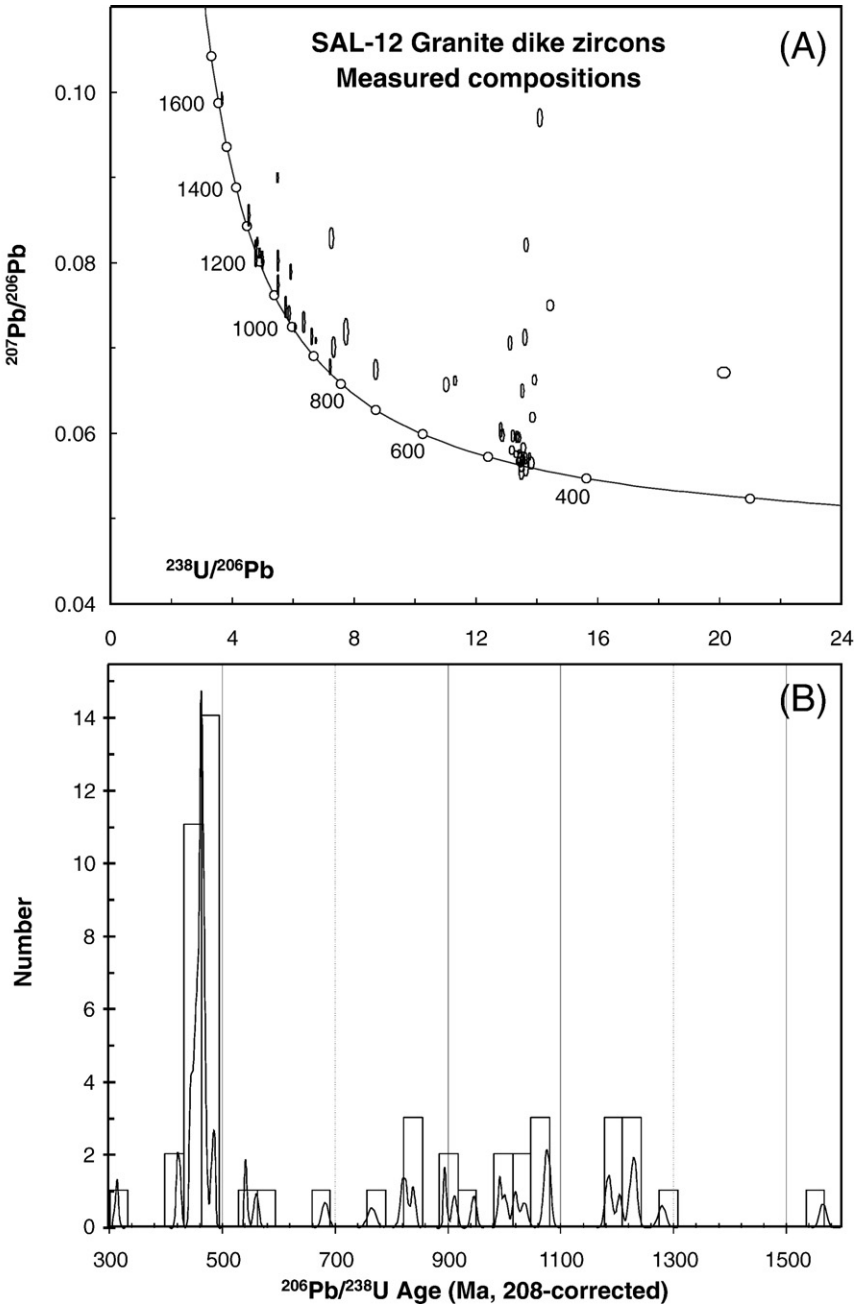

Fig. 7. U–Pb LA-ICPMS zircon analyses from granitic dike cutting the Amate Unit (sample SAL-12) plotted on (A) a Terra–Wasserburg diagram, and (B) a histogram.

The Salada Unit, in addition to these latter populations also contains ~352 Ma detrital zircons. Such ages (353–346 Ma) have been recorded in the zircons from eclogites of the Piaxtla Suite in the central part of the Acatlán Complex (Middleton et al., 2007; Elías-Herrera et al., 2007), where they have been related to exhumation of subduction-related rocks. Thus a local source is likely, however by this time, Pangea had amalgamated and thus more distal sources are also possible.

6.1. Terminology

The absence of eclogite facies metamorphism in the Xayacatlán area precludes inclusion of the units in this area in the Piaxtla Suite. Furthermore, the term Xayacatlán is so inextricably linked to the Piaxtla Suite (e.g. Vega-Granillo et al., 2007, and references therein) that we introduce the name, Amate Unit, for the sedimentary rocks previously included in the Xayacatlán Formation. Also the differences in ages of the Huerta and Salada units, both of which were previously assigned to the Cosoltepec Formation (Ortega-Gutiérrez, 1975), justifies their separation and redefinition. A sample of the Cosoltepec Formation type section yielded a similar detrital zircon age population to the Salada Unit, however, the youngest $^{206}Pb/^{238}U$ age reported from the type Cosoltepec Formation is ~376 Ma (discordant data: Talavera-Mendoza et al., 2005), slightly older than the 352 Ma age in the Salada Unit. Both the

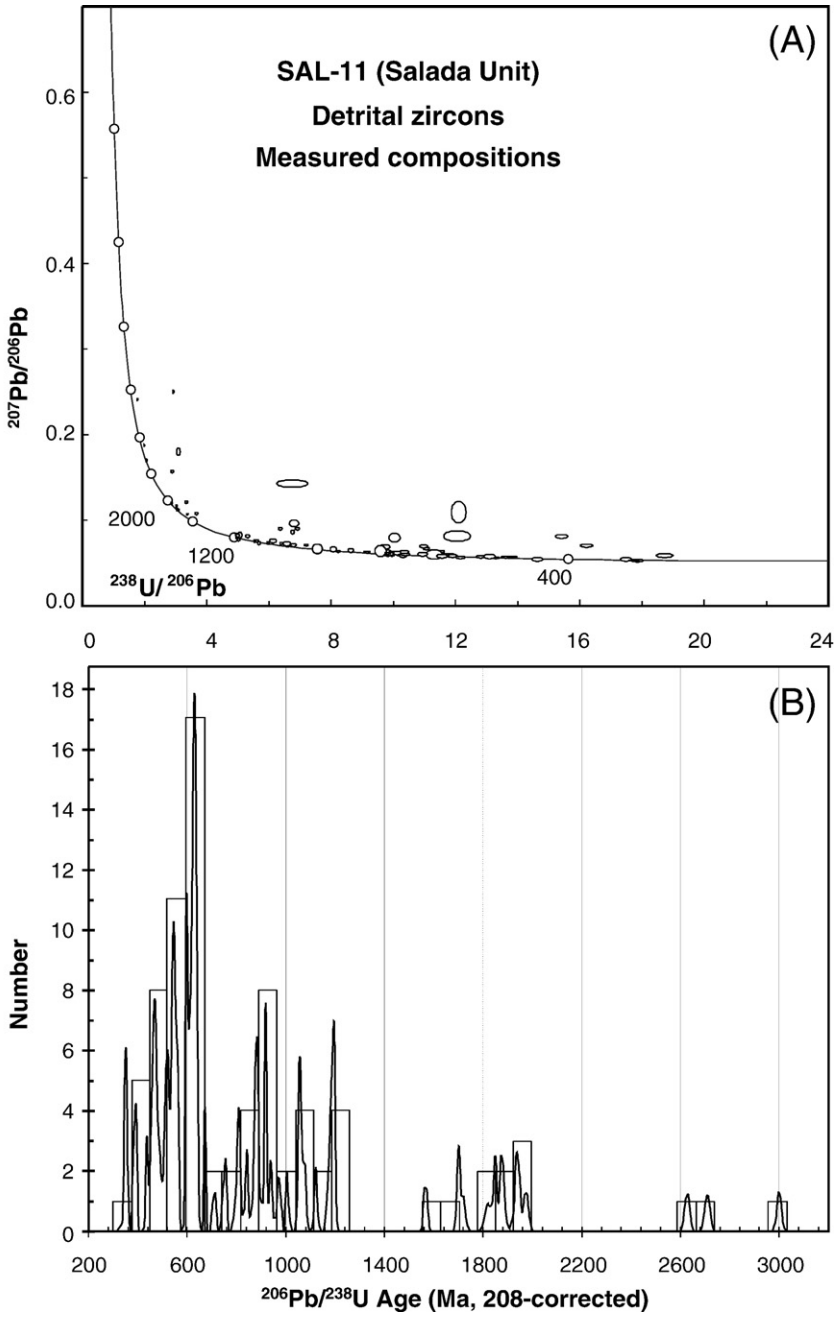

Fig. 8. U–Pb LA-ICPMS zircon analyses from metapsammite of the Salada Unit (sample SAL-11) plotted on (A) a Terra–Wasserburg diagram, and (B) a histogram.

Salada Unit and the type Cosoltepec Formation contain mafic igneous lenses and appear to be continuous along strike from one another (Fig. 1B). However, until mapping and further data confirms their continuity, it is better to maintain the Salada Unit as a distinct unit.

7. Discussion

The younger granitoid rocks dated in the Xayacatlán area, which range from 464±4 Ma to 447±3 Ma age, are very similar to the 442±1 Ma age of a gabbroic dike cutting the Amate Unit (Keppie et al., 2008b). As granitic dikes and pegmatites also cut this mafic dike, it indicates that magmatism in the Xayacatlán area lasted from ~464 Ma to 442 Ma. These igneous rocks are bimodal and the mafic dikes are continental rift tholeiites (Keppie et al., 2008b), and appear to form part of a more widespread ~480–440 Ma magmatic event in the Acatlán Complex. The Huerta Unit appears to have been deposited during this same time interval, and thus it probably represents a rift setting on the margin of Oaxaquia (Fig. 9). The Oaxacan Complex is inferred to have underlain the Acatlán Complex during the Ordovician (Keppie, 2004), an interpretation that is consistent with the ~1 Ga inherited zircons in the pegmatite cutting the Huerta Unit. The same interpretations probably also apply to the Amate Unit, however, it may be somewhat older. The rifted continental margin setting inferred for all of these

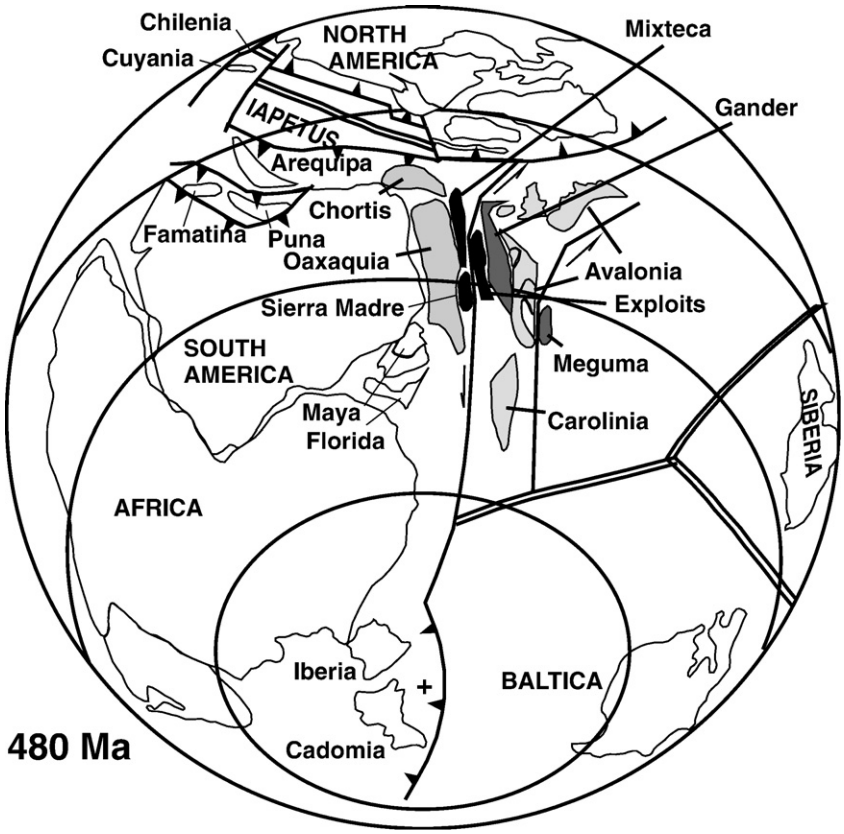

Fig. 9. Ordovician paleogeographic reconstruction showing the location of the Huerta and Amate units on the southern margin of the Rheic Ocean (modified after Keppie, 2004).

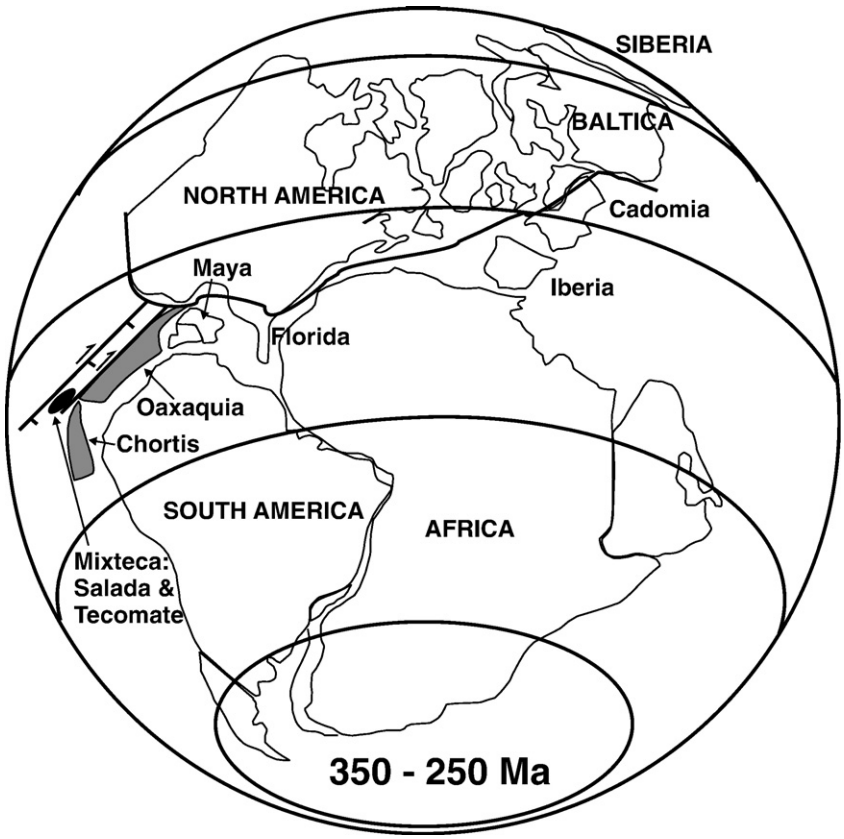

Fig. 10. Carboniferous paleogeographic reconstruction showing the location of the Salada Unit on the western margin of Pangea (modified after Keppie, 2004).

Ordovician (and possibly older) rocks is more consistent with the deposition along the rift-drift southern margin of the Rheic Ocean (Fig. 9), because the Iapetus Ocean was closing during the Ordovician and it was bordered by active margins. Furthermore, all the detrital zircons in these two units could have been derived from Oaxaquia and Amazonia: the Neoproterozoic zircons are incompatible with the derivation from Laurentia.

The presumed Carboniferous age of the Salada Unit suggests that its deposition was synchronous with the older parts of the latest Devonian–Early Permian Patlanaoaya Group (Vachard et al., 2000), which was synchronous with extensional deformation and easterly dipping subduction (Ramos-Arias et al., 2008). The overlying Permian Tecomate Formation was synchronous with arc magmatism (Torres et al., 1999), including the Totoltepec laccolith. That these rocks formed on the western margin of Pangea (Fig. 10) is indicated by the Midcontinent (USA) faunal affinity of fossils in the Mississippian rocks lying on top of the Oaxacan Complex (Navarro-Santillan et al., 2002).

Acknowledgements

We would like to acknowledge a Papiit grant (IN103003) and a CONACyT grant (CB-2005-1: 24894) to JDK. CONACyT contributed to studies for MMG. We are grateful for constructive reviews by Drs. Peter A. Cawood and José R. Martínez Catalán.

References

Campa, M.F., Coney, P.J., 1983. Tectono-stratigraphic terranes and mineral distributions in Mexico. Canadian Journal of Earth Science 20, 1040–1051.

Eggins, S.M., Kinsley, L.P.J., Shelley, J.M.G., 1998. Deposition and element fractionation processes during atmospheric pressure laser sampling for analysis by ICP-MS. Applied Surface Science 127/129, 278–286.

Elías-Herrera, M., Ortega-Gutiérrez, F., 2002. Caltepec fault zone: an Early Permian dextral transpressional boundary between the Proterozoic Oaxacan and Paleozoic Acatlán complexes, southern Mexico, and regional implications. Tectonics 21 (3). doi:10.1029/200TC001278.

Elías-Herrera, M., Macías-Romo, C., Ortega-Gutiérrez, F., Sánchez-Zavala, J.L., Iriondo, A., Ortega-Rivera, A., 2007. Conflicting stratigraphic and geochronologic data from the Acatlán Complex: "Ordovician" granites intrude metamorphic and sedimentary rocks of Devonian–Permian age. Eos Transactions of the American Geophysical Union 88 (23) Joint Assembly Supplement, Abstract T41A-12.

Keppie, J.D., 2004. Terranes of Mexico revisited: a 1.3 billion year odyssey. International Geology Review 46, 765–794.

Keppie, J.D., Ramos, V.S., 1999. Odyssey of terranes in the Iapetus and Rheic Oceans during the Paleozoic. In: Keppie, J.D., Ramos, V.A. (Eds.), Laurentia–Gondwana Connections Before Pangea. Geological Society of America Special Paper, vol. 336, pp. 267–276.

Keppie, J.D., Dostal, J., Cameron, K.L., Solari, L.A., Ortega-Gutiérrez, F., Lopez, R., 2003. Geochronology and geochemistry of Grenvillian igneous suites in the northern Oaxacan Complex, southern México: tectonic implications. Precambrian Research 120, 365–389.

Keppie, J.D., Sandberg, C.A., Miller, B.V., Sánchez-Zavala, J.L., Nance, R.D., Poole, F.G., 2004a. Implications of latest Pennsylvanian to Middle Permian paleontological and U–Pb SHRIMP data from the Tecomate Formation to re-dating tectonothermal events in the Acatlán Complex, southern Mexico. International Geology Review 46, 745–753.

Keppie, J.D., Nance, R.D., Powell, J.T., Mumma, S.A., Dostal, J., Fox, D., Muise, J., Ortega- Rivera, A., Miller, B.V., Lee, J.W.K., 2004b. Mid-Jurassic tectonothermal event superposed on a Paleozoic geological record in the Acatlán Complex of southern Mexico: hotspot activity during the breakup of Pangea. Gondwana Research 7, 239–260.

Keppie, J.D., Nance, R.D., Fernández-Suárez, J., Storey, C.D., Jeffries, T.E., Murphy, J.B., 2006. Detrital zircon data from the eastern Mixteca terrane, southern Mexico: evidence for an Ordovician–Mississippian continental rise and a Permo-Triassic clastic wedge adjacent to Oaxaquia. International Geology Review 48, 97–111.

Keppie, J.D., Dostal, J., Murphy, J.B., Nance, R.D., 2008a. Synthesis and tectonic interpretation of the westernmost Paleozoic Variscan orogen in southern Mexico: from rifted Rheic margin to active Pacific margin. Tectonophysics.

Keppie, J.D., Dostal, J., Ramos-Arias, M.A., Morales-Gámez, M., Miller, R.D., Nance, Murphy, J.B., Ortega-Rivera, A., Lee, J.W.K., 2008b. Ordovician rift tholeiites in the Acatlán Complex, southern Mexico: evidence of rifting on the southern margin of the Rheic Ocean. Tectonophysics.

Malone, J.W., Nance, R.D., Keppie, J.D., Dostal, J., 2002. Deformational history of part of the Acatlán Complex: Late Ordovician–Early Silurian and Early Permian orogenesis in southern Mexico. Journal of South American Earth Sciences 15, 511–524.

Middleton, M., Keppie, J.D., Murphy, J.B., Miller, B.V., Nance, R.D., Ortega-Rivera, A., Lee, J.K.W., 2007. P–T–t constraints on exumation following subduction in the Rheic Ocean from eclogitic rocks in the Acatlán Complex of southern Mexico. In: Linnemann, U., Nance, R.D., Kraft, P., Zulauf, G. (Eds.), The Evolution of the Rheic Ocean: From Avalonian–Cadomian Active Margin to Alleghenian–Variscan Collision. Geological Society of America Special Paper, vol. 423, pp. 489–509.

Miller, B.V., Dostal, J., Keppie, J.D., Nance, R.D., Ortega-Rivera, A., Lee, J.W.K., 2007. Ordovician calc-alkaline granitoids in the Acatlán Complex, southern Mexico: geochemical and geochronological data and implications for tectonic of the Gondwanan margin of the Rheic Ocean. In: Linnemann, U., Nance, R.D., Zulaf, G., Kraft, P. (Eds.), The Evolution of the Rheic Ocean: From Avalonian–Cadomian Active Margin to Alleghenian–Variscan Collision. Geological Society of America Special Paper, vol. 423, pp. 465–475.

Nance, R.D., Miller, B.V., Keppie, J.D., Murphy, J.B., Dostal, J., 2006. The Acatlán Complex, southern Mexico: record of Pangea assembly to breakup. Geology 34, 857–860.

Nance, R.D., Miller, B.V., Keppie, J.D., Murphy, J.B., Dostal, J., 2007. Vestige of the Rheic Ocean in North America: the Acatlán Complex of southern México. In: Linnemann, U., Nance, R.D., Zulaf, G., Kraft, P. (Eds.), The Evolution of the Rheic Ocean: From Avalonian–Cadomian Active Margin to Alleghenian–Variscan Collision. Geological Society of America Special Paper, vol. 423, pp. 437–452.

Navarro-Santillan, D., Sour-Tovar, F., Centeno-Garcia, E., 2002. Lower Mississippian (Osagean) brachiopods from the Santiago Formation, Oaxaca, Mexico: stratigraphic and tectonic implications. Journal of South American Earth Sciences 15, 327–336.

Ortega-Gutiérrez, F., 1975. The pre-Mesozoic geology of the Acatlán area, south Mexico: Ph.D. thesis, Leeds University, U.K.166 pp.

Ortega-Gutiérrez, F., Elias-Herrera, M., Reyes-Salas, M., Macias-Romo, C., López, R., 1999. Late Ordovician–Early Silurian continental collision orogeny in southern Mexico and its bearing on Gondwana–Laurentia connections. Geology 27, 719–722.

Ortega-Obregón, C., Keppie, J.D., Solari, L.A., Ortega-Gutiérrez, F., Dostal, J., López, R., Ortega-Rivera, A., Lee, J.W.K., 2003. Geochronology and geochemistry of the ~917 Ma, calc-alkaline Etla granitoid pluton (Oaxaca, southern México): evidence of post-Grenvillian subduction along the northern margin of Amazonia. International Geology Review 45, 596–610.

Paces, J.B., Miller, J.D., 1993. Precise U-Pb ages of the Duluth Complex and related mafic intrusions, northeastern Minnesota: geochronological insights to physical, petrogenetic, paleomagnetic, and tectonomagmatic processes associated with the 1.1 Ga Midcontinent Rift System. Journal of Geophysical Research 98, 13997–14013.

Ramírez-Espinosa, J., 2001. Tectono-magmatic evolution of the Paleozoic Acatlán Complex in southern Mexico, and its correlation with the Appalachian system: Ph.D. thesis, University of Arizona, 170 p.

Ramos-Arias, M.A., Keppie, J.D., Ortega-Rivera, A., Lee, J.W.K., 2008. Extensional deformation on the western margin of Pangea, Patlanoaya area, Acatlán Complex, southern Mexico. Tectonophysics.

Sánchez-Zavala, J.L., Ortega-Gutiérrez, F., Elías-Herrera, M., 2000. La orogenia Mixteca del Devónico del complejo Acatlán, sur de México. GEOS Unión Geofísica Mexicana, Boletin Informativo Época II, 20, No. 3, pp. 321–322.

Sánchez-Zavala, J.L., Ortega-Gutiérrez, F., Keppie, J.D., Jenner, G.A., Belousova, E., Maciás-Romo, C., 2004. Ordovician and Mesoproterozoic zircons from the Tecomate Formation and Esperanza granitoids, Acatlán Complex, southern Mexico: local provenance in the Acatlán and Oaxacan complexes. International Geology Review 46, 1005–1021.

Solari, L.A., Keppie, J.D., Ortega-Gutiérrez, F., Cameron, K.L., Lopez, R., Hames, W.E., 2003. ~990 and ~1,100 Grenvillian tectonothermal events in the northern Oaxacan Complex, southern Mexico: roots of an orogen. Tectonophysics 365, 257–282.

Talavera-Mendoza, O., Ruíz, J., Gehrels, G.E., Meza-Figueroa, D.M., Vega-Granillo, R., Campa-Uranga, M.F., 2005. U–Pb geochronology of the Acatlán Complex and implications for the Paleozoic paleogeography and tectonic evolution of southern Mexico. Earth and Planetary Science Letters 235, 682–699.

Torres, R., Ruíz, J., Patchett, P.J., Grajales-Nishimura, J.M., 1999. Permo-Triassic continental arc in eastern Mexico; tectonic implications for reconstructions of southern North America. In: Bartolini, C., Wilson, J.L., Lawton, T.F. (Eds.), Mesozoic Sedimentary and Tectonic History of North-central Mexico. Geological Society of America Special Paper, vol. 340, pp. 191–196.

Vega-Granillo, R., Talavera-Mendoza, O., Meza-Figueroa, D., Ruiz, J., Gehrels, G.E., López-Martínez, M., de La Cruz-Vargas, J.C., 2007. Pressure–temperature–time evolution of Paleozoic high-pressure rocks of the Acatlán Complex (southern Mexico): implications for the evolution of the Iapetus and Rheic Oceans. Geological Society of America Bulletin 119, 1249–1264.

Vachard, D., Flores de Dios, A., Pantoja, J., Buitrón, B.E., Arellano, J., Grajales, M., 2000. Les fusulines du Mexique, une revue biostratigraphique et paléogéographique. Geobios 33, 655–679.

Yañez, P., Ruiz, J., Patchett, J.P., Ortega-Gutiérrez, F., Gehrels, G.E., 1991. Isotopic studies of the Acatlán Complex, southern Mexico: implications for Paleozoic North American tectonics. Geological Society of America Bulletin 103, 817–828.